8-24-2011

Automation of Orthodontic Wire Tester for Performing Three Point Bending Tests

Adithya Venkatesan
adithya1987@gmail.com

AUTOMATION OF ORTHODONTIC WIRE TESTER FOR PERFORMING THREE POINT BENDING TESTS

Adithya Venkatesan

B.Tech, SASTRA University, 2008

A Thesis

Submitted in Partial Fulfillment of the

Requirements for the Degree of

Master of Science

At the

University of Connecticut

August 2011

APPROVAL PAGE

Master of Science Thesis

AUTOMATION OF ORTHODONTIC WIRE TESTER FOR PERFORMING THREE POINT BENDING TESTS

Presented by

Adithya Venkatesan, B.Tech.

Major Advisor _____

Donald R. Peterson

Associate Advisor _____

Ravindra Nanda

Associate Advisor _____

Flavio Uribe

University of Connecticut

August 2011

Acknowledgments

I would like to thank Dr. Donald Peterson for giving me this opportunity to work in this project and for constantly supporting the research conducted for completion of this thesis. I would also like to thank Dr. Ravindra Nanda and Dr. Flavio Uribe for their valuable inputs in making me understand the principles of orthodontics.

The students and staff of the Biodynamics Laboratory all provided valuable support to complete this project. Takafumi Asaki helped me in every phase of the project and was always willing to provide feedback to help diagnose and debug the inevitable problems.

Finally, I would like to thank my parents and brother for encouraging me to meet my full academic potential and pursue a Master's degree in engineering. Without their continued support at home, I would not be able to maintain the quality and effort that went into my research.

Table of Contents

List of Figures

List of Tables

Abstract

Understanding the biomechanical factors in orthodontics is important in order to improve the overall effectiveness of actual clinical treatment. An accurate method to study the three-dimensional (3D) force systems and the resulting movements of teeth during orthodontic treatment is needed along with the understanding of the material properties of any orthodontic wire. Until recently, most of the orthodontic biomechanics literature was limited to two-dimensional experimental studies. Recent advances in three-dimensional computer modeling have also been developed but have been limited to the manual control of tooth movement. Overall, there is very little published evidence in the literature on the measurement and analysis of three-dimensional orthodontic force systems.

The purpose of this thesis was to develop a cost-effective orthodontic wire tester that is capable of three-dimensional measurements and analyses of orthodontic force systems. A device was developed that can perform standardized three point bending tests on any orthodontic wire according to the International (ISO 15841) and American (ANSI Specification No. 32) standards. Jacobian transformations were validated and were used to measure the force/torque values at precise locations using two three-dimensional force/torque sensors and a stepper motor in a temperature controlled environment. The measurement error of both force/torque sensors was found to be 0.5% or less after extensive verification. As an application, the load/displacement curves for six different sizes of Nickel-Titanium (Ni-Ti) wires were generated using a three bending test protocol, which was developed in LabVIEW. To further validate the efficacy of the device, the unloaded bending force values were compared with the manufacturer's

specifications and the results showed a high degree of correlation. A comparative study between the standardized three point bending test of ISO and ANSI was also performed and demonstrated good measurement correlation between these standards.

The successful development of the orthodontic wire tester, including its computer protocols, will allow orthodontists to determine, with great accuracy, the forces and torques acting at precise locations on the teeth. It will also allow for future simulation research on new and existing orthodontic clinical applications by orthodontists and biomedical engineers.

1. Introduction

Orthodontics is the specialty of dental medicine, which deals with the study and treatment of tooth irregularity. An understanding of several fundamental mechanical concepts (see Section 1.1) is essential in order to understand the clinical relevance of biomechanics to orthodontics. The treatment (see Section 1.2) focuses on tooth movement which results from the application of forces to the teeth. These forces are produced by various appliances (wires, brackets, elastics, etc.) inserted and activated by the clinician. Teeth and the associated support structures respond to these forces with complex biological reactions, resulting in tooth movement. Understanding the material properties of the wire is an important task for the orthodontists in order to achieve a precise biological response before applying it to the patients.

The three point bending test (see Section 1.3) provides information on these properties. Minimizing or eliminating the unknown factors related to the delivery of treatment can reduce the variability in the treatment response and the knowledge of the mechanical principles governing these forces are necessary for the control of orthodontic treatment. Though a wide variety of research methods (see Section 1.5) had been employed to study the clinical application of biomechanical concepts, the fundamental problem is the difficulty in implementing the theoretical knowledge in everyday orthodontics. This difficulty rests in the lack of suitable methods available for objective control of the force-moment systems applied during therapy.

Using the recent advances in six degrees of freedom (DOF) sensors and other technologies, this thesis details the development of a cost-efficient Orthodontic Wire Tester capable of performing three point bending test and real-time measurement of all

the six degrees of freedom exactly at the location of teeth. Eventually, this system will be used in future orthodontic research to understand several clinical issues at the University of Connecticut Health Center.

1.1 Fundamental mechanical concepts

The first concept, Center of Resistance, states that, for a free object to move linearly without any rotation, the applied force must pass through the center of mass. Center of resistance of a tooth is dependent on the root length and morphology, the number of roots, and the level of alveolar bone support (Nanda et al., 2005). The exact location of the center of resistance for a tooth is not easily identified; however, analytical studies have determined that the center of resistance for single rooted teeth with normal alveolar bone levels is about one-fourth to one-third the distance from the cemento-enamel junction to the root apex. Determination of the horizontal, vertical, and transverse components of a force improves the understanding of the direction of tooth movement that might be expected.

The moment of the force results in some rotational movement (Lindauer, 2001). Awareness of the moment of the force is needed to develop effective and efficient appliance designs. Tooth movement can be described in many ways. The potentially infinite variety of movements can be categorized into basic types: tipping, translation, root movement, and rotation. Each type of basic movement is the result of variation of the applied moment and the force. The relationship between the applied force system and the type of movement can be described by the moment-to-force (M/F) ratio. The M/F ratio of the applied force and moment determines the type of rotational movement. A tooth's response to a force can be studied at three levels: clinical, cellular, and

biomechanical. The clinical level allows the study of phenomena such as rate and direction of tooth movement, pain response, and tooth mobility. The cellular level gives insight into biology behind the tooth movement, including the dynamics of bone and connective tissue. The vaguely understood biomechanical level provides the ability to accurately determine the level of stress in various areas of the periodontal ligament (PDL); this might be the best means of correlating the application of a force on a tooth with the tooth's response (Garreck et al., 2003).

1.2 Application of force and treatment methods

Arch-wires ideally are designed to move teeth with light continuous forces. They are placed through the brackets and retained in position using ligatures and elastic module. Arch-wires, springs, and elastics are the primary means of generating forces for orthodontic treatment.

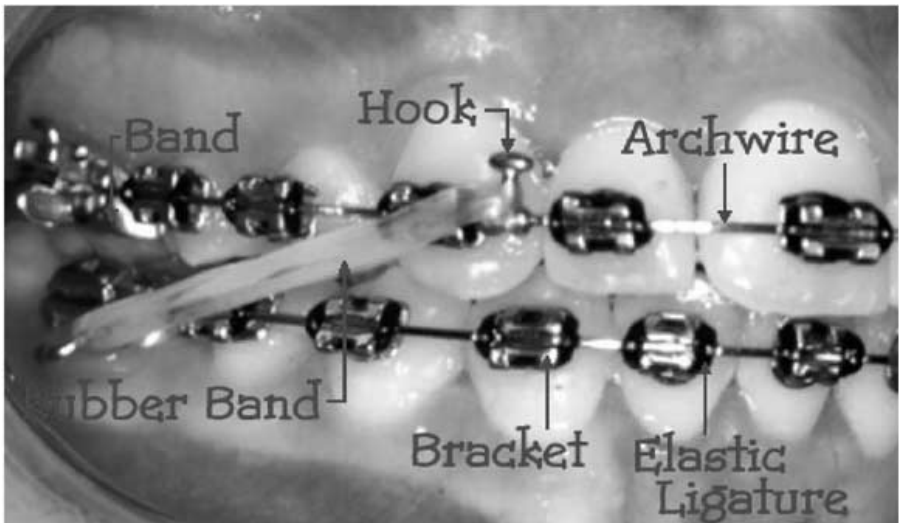

Figure 1: Representation of Brackets, Arch-wire, Elastic Ligature (Huang et al., 2003)

Orthodontic wires are specifically designed for the application of force on a tooth. There are many different kinds of orthodontic wires, designed for specific force applications. In order to optimize the biological environment for tooth movement and minimize patient's discomfort, selection of these wires plays a vital role. Oltjen et al., (1995) stated that wires of low stiffness that are used to produce gentle forces to teeth are leveled and aligned. The wire is worked into a linear shape by a mechanical straightening method, in order to correct waviness of the wire resulting from the final cold reduction. This wire is then kept at a temperature of 500 through 600 degree celsius in order to provide high mechanical strength, excellent corrosion resistance, and superior toughness (Iijima et al., 2002). The wires and springs are fabricated from a myriad of alloys. The standard materials used are stainless steel, nickel–titanium alloys, titanium–molybdenum alloys and variety of other alloys (Burstone, 1984). Orthodontic treatment is usually divided into three phases, namely, leveling and aligning, space closure, detailing and finishing. Each phase requires a particular type of wire with desired characteristics.

The mechanical characteristics of a material are determined by several factors. Intrinsic properties are inherent qualities of the wire. These properties are determined by the material composition at a molecular or crystalline level (Walker et al., 2007). Variation of intrinsic properties alters the nature of the alloy itself. Extrinsic properties are macroscopic features of the material such as wire diameter or length.

The ideal requirement of arch-wire is strength, stiffness, biocompatibility, coefficient of friction, resilience, and super elasticity. Each of these properties plays a major role in the application of force and the resulting teeth movement. Some of the common materials used for making orthodontic wires are stainless steel, nickel,

chromium, titanium, and carbon. Specific alloy compositions will lead to unique properties of wire.

Brackets are another important factor that influence the application of force to the teeth (Bedner et al., 1999). Wide variety of research is being performed to understand the force transfer to the teeth from the wires. They are the slots in the teeth over which orthodontic wires are attached. The contact between these two lead to frictional losses. Clinicians bend the wires to create a strain and they assume that certain amount of force would be transferred to the teeth due to the bend. Due to the contact between the brackets, wires and elastics some amount of forces are being lost. There are different kinds of brackets available in markets with different characteristics.

Ideal orthodontic treatment achieves specific, individualized, predetermined treatment objectives (Nanda et al., 2005). Three major components of the treatment are diagnosis–identifying the patient's specific problems which require treatment, treatment planning–establishing treatment objectives to solve the problem, delivering treatment – the course of action selected that addresses the patient's problems directed toward meeting the individualized goals. These components imply that treatment requirements will vary for each patient. Hence a single appliance design (bracket prescription, arch-wire sequence, etc.) cannot be used uniformly with all patients. Ideal treatment requires forces to be within an appropriate range to show an efficient biological response without any side effects (Kapila et al., 1991). An optimal force is the lightest force that will move a tooth to a desired position in the shortest possible time and with minimal side effects. Force constancy is the consistency of the applied force over the range of activation of the appliance. For tooth movements over large distances, the continuity of the force levels

throughout is often desired. Force constancy can be obtained by reducing the load-deflection rate in one or more of the following ways: reducing the cross-section of a wire, increasing the inter-bracket distance, incorporating loops in the wire and using memory alloys. Reducing the cross-section of a wire is commonly used to improve the force constancy and to reduce the load-deflection rate. The advantage of using small-diameter wires is that, flexibility eases ligation into the brackets, especially at the earlier stages of the treatment when the teeth are misaligned. Large inter attachment distance reduces the load-deflection rate and helps deliver constant force magnitude, providing a better directional control of the tooth movement. Incorporating loops into the appliance system increases the wire material, thereby reducing the load-deflection rate. One of the significant advances in the practice of orthodontics has been the introduction of memory alloys such as nickel titanium to effectively reduce the load-deflection rate (Kasuya, 2007). The nickel-titanium wire has a significantly lower modulus of elasticity than the stainless steel wires. A reduction in the modulus of elasticity translates into an almost 1:1 reduction in the load-deflection of the arch-wire.

The point of force application is a very important fundamental consideration in the appliance design. The point of force delivery and direction of the force relative to the center of resistance of tooth have a significant effect on the type of tooth movement. Forces acting at a distance from the center of resistance generate moments of the force, potentially producing unwanted tooth movements. These biomechanical principles are of fundamental importance to understanding orthodontic treatment. This makes a necessity to develop a device used particularly for determining the biomechanical factors involved in orthodontic treatment.

1.3 Three point bending test

They are the most commonly used testing procedure to characterize the mechanical properties of the materials. There has been lot of research on three point bending test as it evaluates the load-deflection properties, which are considered the most important parameters determining the biological nature of tooth movement according to Krishnan and Kumar (2004). Kapila et al., (1992) suggested that the inherent tendency of the wire on loading is to try to return to its original shape or to unload. This unloading of the wire provides the force required to cause biologic tissue response, which tends to move the tooth into alignment. The loading portion of the graphs obtained from three point bending test simulates the activation of the wire, whereas the unloading segment of the graph provides some information on forces associated with the wire as it undergoes deactivation. Therefore, the unloading forces associated with the wire provide some indication of its potential clinical behavior.

The biggest advantages of this test are it closely simulates to clinical application and its ability to differentiate wires with super elastic properties (Krishnan et al., 2004). Wilkinson et al., (2002) mentioned that it also offers a high degree of reproducibility which facilitates comparison between different studies.

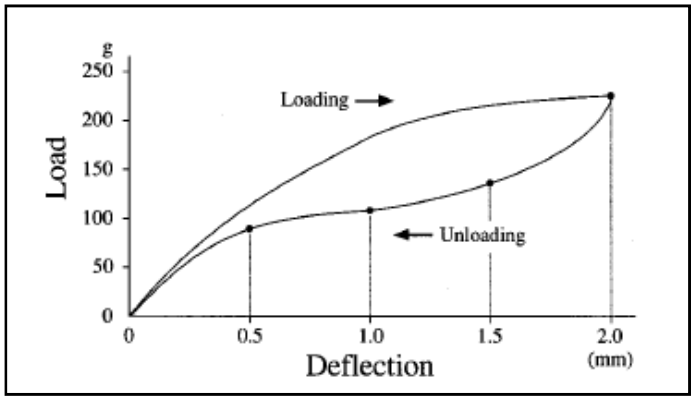

Figure 2: Schematic load-deflection curve (Nakanu et al., 1999)

In Figure 2, Nakanu et al., (1999) described load-deflection curve for several Ni-Ti wires. There are several different strategies adopted for developing three point bending test apparatus by previous researchers. Theodosia et al., (2007) analyzed load- deflection characteristics of superelastic Nickel-Titanium (Ni-Ti) wires by three point bending test using universal testing machine (INSTRON 4444; Instron, Canton, Mass).

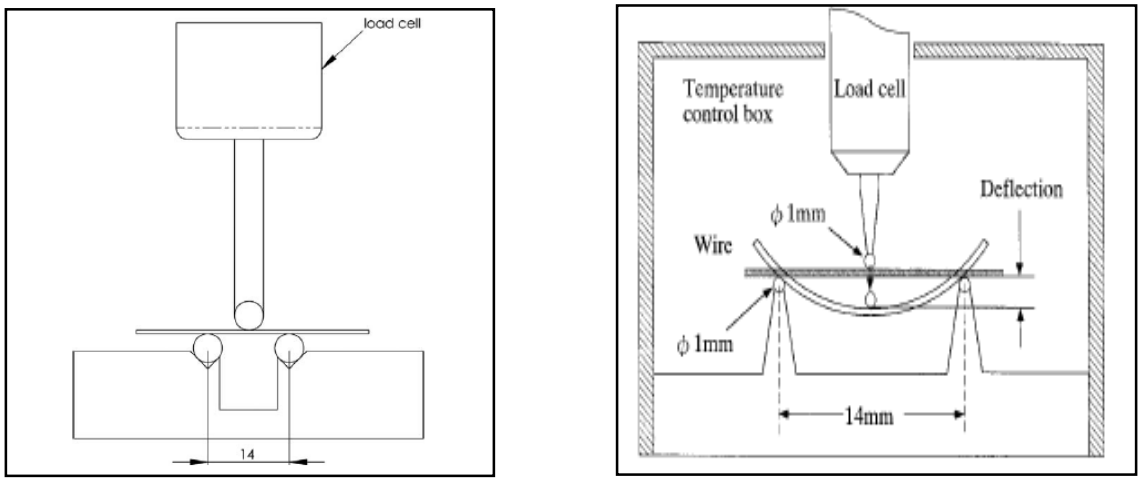

A) B)

Figure 3: A) Intron model (Theodosia et al., 2007), B) Bending model (Nakanu et al., 1999)

Oltjen et al., (1997) used a stylus, which was connected to the crosshead of an Instron universal testing (Model # 1135, Instron Corporation, Canton, and Mass) and centered at midspan of each wire specimen. They used a data acquisition device (Model # CIO-DAS08-PGL, Omega Engineering Inc, Stamford, Conn) for acquiring voltage from the load cell. The span length shown in Figure 3 is 14mm, which is considered to be the inter bracket distance between the central incisor and canine.

There are two standard testing protocols, ISO and ANSI standards, to perform this test. The difference in setup between ANSI and ISO is illustrated in Figure 4. Apart from

setup there are few other differences in the testing procedure which are mentioned in Table 1.

Table 1: Difference in test methods of ANSI and ISO testing

Test Methods		
Specifications	ISO	ANSI
Specimen size(mm)	30	50
Speed(mm/min)	7.5±2.5	10
Span length(mm)	10	12
Temperature(Celsius)	36±1	36±1

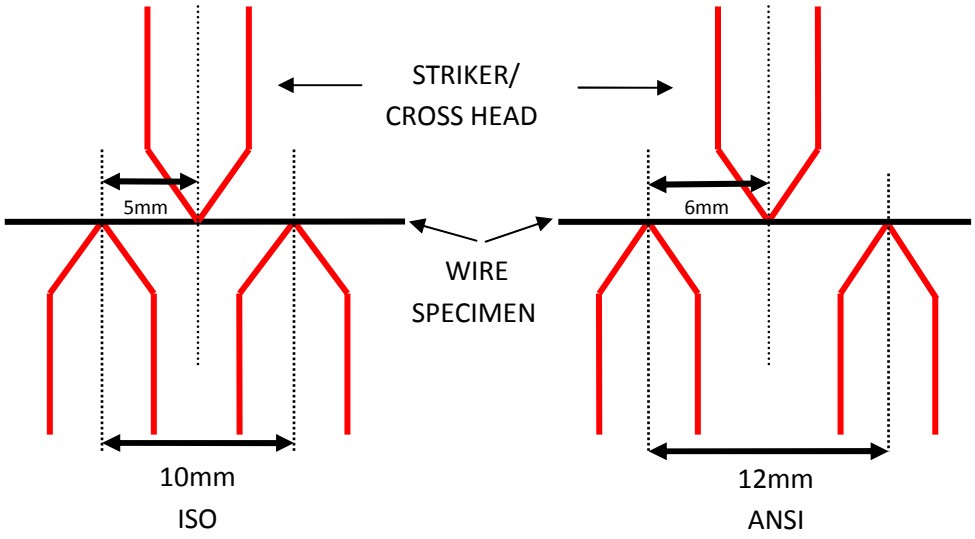

Figure 4: Simple 3pt bending test set up

The striker can be moved up and down manually by a screw or it can be controlled by a motor. The relationship between the applied force and the deflection under three-point bending conditions is given by Equation (1),

$$F = \frac{48EID}{L^3}, \qquad (1)$$

Where **F** is the applied force by the striker, **E** is the elastic modulus of the material, **D** is the deflection, **I** is the moment of inertia of the cross section, **L** is the length span of the two points (Kusy et al., 1984). This relationship is useful for comparing the relative values of forces in bending for arch-wires. After analyzing the importance of three point bending test, there was a necessity to incorporate this testing methods into orthodontic wire tester.

1.4 Jacobian transformations

Assuming a force and moment acting at the origin of some coordinate frame attached to a fixed object, the equivalent force and moment acting with respect to some other coordinate frame, which is also attached rigidly to the object, could be determined using this transformations. The Jacobian operations are necessary to transform force systems from load cell frame to tooth frame, since the size of the load cell and tooth are different. This thesis details the validation of the Jacobian matrix and how these operations allow calculating the force and moment exactly at the location of teeth. Badawi et al., (2009) demonstrated the use of Jacobian matrix to transform the force systems exactly at the location of teeth. To perform those transformations accurately they demonstrated the importance of accurately knowing the X, Y, and Z coordinates and the orientation of tooth with respect to the designated load cell. Hiromichi et al., (1999) developed [6×6] Jacobian matrix which allowed transformation for forces and moments from the sensor coordinate system to the joint coordinate system. Paul (1981) demonstrated the detailed derivation of Jacobian matrix, which consists of a number of matrix operations. In order to derive Jacobian matrix, it is important to understand the concept of transformation. Transformation of space **H** is a [4×4] matrix which can

represent translation, rotation movements. Given a point **U**, its transformation **V** is represented by the matrix product (Equation (2)).

$$\mathbf{V=HU} \tag{2}$$

The transformation **H** corresponding to translation by vector a**i** + b**j** + c**k** is given by Equation (3),

$$\mathbf{H=Trans(a,b,c)} = \begin{bmatrix} 1 & 0 & 0 & a \\ 0 & 1 & 0 & b \\ 0 & 0 & 1 & c \\ 0 & 0 & 0 & 1 \end{bmatrix} \tag{3}$$

The transformation corresponding to rotations about the x, y, and z axis by an angle θ are explained by Equations (4), (5) and (6),

$$\mathbf{Rot(x,\theta)}= \begin{bmatrix} 1 & 0 & 0 & 0 \\ 0 & \cos\theta & -\sin\theta & 0 \\ 0 & \sin\theta & \cos\theta & 0 \\ 0 & 0 & 0 & 0 \end{bmatrix} \tag{4}$$

$$\mathbf{Rot(y,\theta)}= \begin{bmatrix} \cos\theta & 0 & \sin\theta & 0 \\ 0 & 1 & 0 & 0 \\ -\sin\theta & 0 & \cos\theta & 0 \\ 0 & 0 & 0 & 1 \end{bmatrix} \tag{5}$$

$$\mathbf{Rot(z,\theta)}= \begin{bmatrix} \cos\theta & -\sin\theta & 0 & 0 \\ \sin\theta & \cos\theta & 0 & 0 \\ 0 & 0 & 1 & 0 \\ 0 & 0 & 0 & 1 \end{bmatrix} \tag{6}$$

If both translation and rotation occur, the transformation **H** is the product of rotational and translational matrix as shown in Equation (7).

$$\mathbf{H = Rot(\ ) \times Trans(\ )} \tag{7}$$

General notation of **H** is given by Equation (8)

$$\mathbf{H}= \begin{bmatrix} n_x & o_x & a_x & p_x \\ n_y & o_y & a_y & p_y \\ n_z & o_z & a_z & p_z \\ 0 & 0 & 0 & 1 \end{bmatrix} \tag{8}$$

Jacobian matrix is [6 × 6] given by Equation (9)

$$\mathbf{J}=\begin{bmatrix} \mathbf{n_x} & \mathbf{n_y} & \mathbf{n_z} & \mathbf{(p\times n)_x} & \mathbf{(p\times n)_y} & \mathbf{(p\times n)_z} \\ \mathbf{o_x} & \mathbf{o_y} & \mathbf{o_z} & \mathbf{(p\times o)_x} & \mathbf{(p\times o)_y} & \mathbf{(p\times o)_z} \\ \mathbf{a_x} & \mathbf{a_y} & \mathbf{a_z} & \mathbf{(p\times a)_x} & \mathbf{(p\times a)_y} & \mathbf{(p\times a)_z} \\ \mathbf{0} & \mathbf{0} & \mathbf{0} & \mathbf{n_x} & \mathbf{n_y} & \mathbf{n_z} \\ \mathbf{0} & \mathbf{0} & \mathbf{0} & \mathbf{o_x} & \mathbf{o_y} & \mathbf{o_z} \\ \mathbf{0} & \mathbf{0} & \mathbf{0} & \mathbf{a_x} & \mathbf{a_y} & \mathbf{a_z} \end{bmatrix} \quad (9)$$

Where **n**, **o, a** are the column vectors of the transformation matrix as shown in Equations (10),(11) and (12), in which **n** corresponds to 1st column, **o** corresponds to 2nd column and **a** corresponds to 3rd colum n.

$$\mathbf{n}=\mathbf{n_x i}+\mathbf{n_y j}+\mathbf{n_z k} \quad (10)$$

$$\mathbf{o}=\mathbf{o_x i}+\mathbf{o_y j}+\mathbf{o_z k} \quad (11)$$

$$\mathbf{a}=\mathbf{a_x i}+\mathbf{a_y j}+\mathbf{a_z k} \quad (12)$$

1.5 Previous wire testers

The orthodontic wire mechanical system tester is an innovative product that will combine a machine with new cutting-edge technology to create a device that will serve as an integral role in orthodontic research. While there are many tension and torsion testers out on the market, none are specifically designed for orthodontic measurements, and they lack some essential capabilities like measurement range and cross head speed. The orthodontic wire mechanical system tester will aim to accurately mimic the mechanical systems within the mouth while providing measurements of tension and torsion on three planes.

An apparatus that was able to measure unipolar force systems that was earlier considered to be first generation wire tester was developed by Burstone et al., (1976). A further development of their experimental arrangement was mentioned by Hershey et al.,

(1981). But in neither case it was possible to simulate a certain movement as a reaction to a given force system or to perform spatial measurements (Bourauel,1991). Many researchers developed this device into 2D force systems, using which experimental studies of the biomechanical aspects were performed. According to Lapatki et al., (2007), the clinical situation could be modeled by subdividing the dental arch into two units. This subdivision was based on whether the multiple-point force application occurs only at one or both units. The clinician encounters a complicated and awkward scenario when forces and moments are exerted at multiple locations on the dental arch, as that is the case with the straight-wire appliance (Lapatki 2007). As a consequence, unwanted side effects (e.g., tooth movements in the wrong direction or occlusal-plane canting) may easily develop. Bouraurel et al., (1991) developed an experimental apparatus for the simulation of three-dimensional movements in orthodontics. Several systems for determining all six force moment components at single teeth have been introduced and applied in evaluating force-moment systems in the laboratory and simulating orthodontic treatment (Friedrich et al., 1999).

To study the orthodontic force system in three dimensions, one would need a force sensor capable of measuring 3D forces and moments. Badawi et al., (2009) developed a laboratory-based human model to study the effect of malocclusion of high canine on incisors and premolars using 14 three-dimensional sensors. Measurements were made on all teeth in a dental arch simultaneously. They manually controlled the movement of teeth using a micrometer. There are many wire testers in the market but one had multifunctional capabilities. Previous wire testers were never capable of performing three point bending tests.

1.6 Objectives

Aim of this study is to use two 3D force/torque sensors and a stepper motor to design a cost-effective orthodontic wire tester which can be capable of performing three point bending test, and variety of other clinical orthodontic testing protocols under controlled temperature conditions. Figure 5 details the overview of the objectives of this thesis.

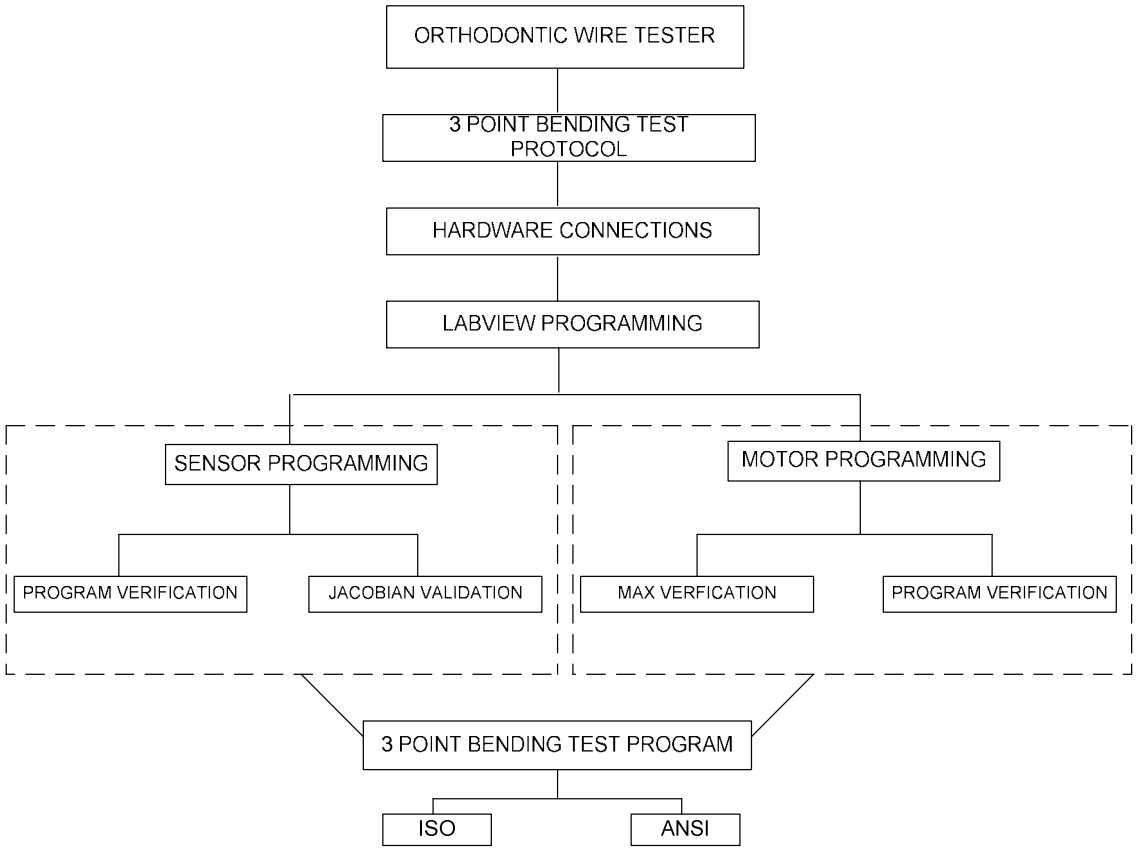

Figure 5: Complete overview of my objectives

2. Methods

2.1 Mechanical components of wire tester

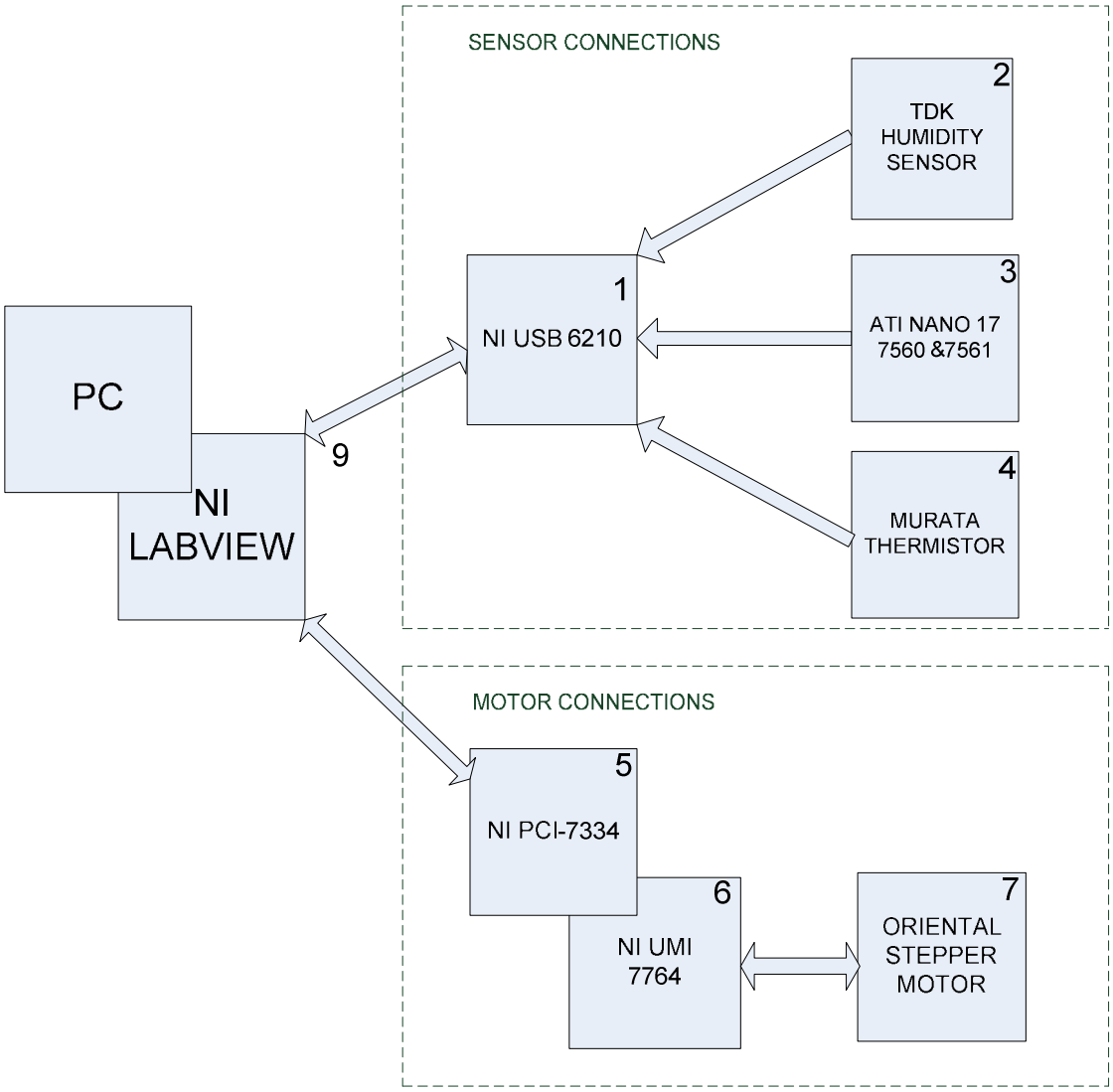

Figure 6: Schematic diagram of hardware components

It was important to understand the major mechanical components of the orthodontic wire tester to develop the automation. National Instrument (NI) USB 6210 Data acquisition device, ATI Nano 17 S/N 7560 & 7561 Force/Torque Sensor, TDK's Humidity Sensor, Murata's Thermistor, NI PCI 7334 , NI UMI 7334, Oriental Stepper

Motor, and Personal Computer were the major mechanical components of orthodontic wire tester and were connected to each other as illustrated in Figure 6.

The NI USB 6210 is the interface for three sensors; humidity sensor, force torque sensor, and thermistor and are linked to LabVIEW. The NI PCI 7334/UMI 7764 is the interface for stepper motor with LabVIEW. It was important to understand sensor and motors connections for achieving LabVIEW control. The arrows indicated in Figure 7 shows the direction of data flow.

2.1.1 Sensor connections

There are three sensors to be controlled in this device.

- **Two force/torque sensors**: Two load cells from Industrial Automation (ATI NANO 17 SI-50-0.50 7560 & 7651) were used to measure the six degrees of freedom components of the applied loads in this device. These are compact sensors and are currently the smallest commercially available 3D load cell. Silicon strain gauges are used in these sensors to detect changes in forces (F/T transducers without electronics (TWE) manual 2010) .
- **Humidity sensor**: A TDK's CHS series humidity sensors was used in our device since they are compact and extremely simple to apply. They contain the necessary circuitry and there was no need to provide additional control circuitry or perform time-consuming calibration. With simple connection to a power supply, they output DC (V) at 100% relative humidity(H) as shown in Equation (13) (TDK's CHS series humidity sensor manual).

$$\mathbf{H = V \times 100} \tag{13}$$

- **Thermistor**: A Murata NTSDXH103FPB30 thermistor was used to measure the temperature in this device. A voltage divider circuit was created to calculate the resistance of the thermistor. Using the Murata product catalog (i.e., Cat.No.R44E-13), the following Equations were derived:

$$R_{th} = \frac{(V_{out} \times R)}{V_{in} - V_{out}}, \tag{14}$$

where R_{th} is Resistance of Thermistor, V_{out} is output of voltage divider circuit, and V_{in} is the voltage input.

$$T = \frac{1}{\left(\left(\frac{1}{\beta}\right) \times \ln\left(\frac{R_{th}}{R}\right)\right) + \frac{1}{T_o}} - 273.15, \tag{15}$$

where T is the temperature of the device, and β is the Thermistor constant.

The voltage signals generated by the force/torque and humidity sensors were used to measure force and humidity. The output from the voltage divider circuit was used to calculate the temperature of the surroundings using Equations (14) and (15).To measure signals from these sensors, a data acquisition (DAQ) device was needed and acted as the interface between the hardware components and the computer. A USB DAQ 6210 (National Instrument) acquires the signal data and feeds it to the computer. Table 2 shows the pin diagram of sensor connections to the USB DAQ 6210 (TWE manual and NI USB DAQ 6210 user manual).

Table 2: Pin diagram for sensor connections *

PIN ASSIGNMENTS	I/O #	PURPOSE
PFI 0/P0.0 (In)	1	
PFI 1/P0.1 (In)	2	
PFI 2/P0.2 (In)	3	
PFI 3/P0.3 (In)	4	
D GND	5	
PFI 4/P0.1 (In)	6	
PFI 5/P0.2 (In)	7	
PFI 6/P0.3 (In)	8	
PFI 7/P0.4 (In)	9	
	10	
D GND	11	
NC	12	
NC	13	
RESERVED	14	
AI 0	15	Humidity sensor
AI 8	16	Thermistor
AI 1	17	channel 1 (F/T SG0 HIGH S/N 7560)
AI 9	18	channel 1 (F/T SG0 HIGH S/N 7561)
AI 2	19	channel 2 (F/T SG1 HIGH S/N 7560)
AI 10	20	channel 2 (F/T SG1 HIGH S/N 7561)
AI 3	21	channel 3 (F/T SG2 HIGH S/N 7560)
AI 11	22	channel 3 (F/T SG2 HIGH S/N 7561)
AI SENSE	23	
AI 4	24	channel 4 (F/T SG3 HIGH S/N 7560)
AI 12	25	channel 4 (F/T SG3 HIGH S/N 7561)
AI 5	26	channel 5 (F/T SG4 HIGH S/N 7560)
AI 13	27	channel 5 (F/T SG4 HIGH S/N 7560)
AI GND	28	SG0-SG6 LOW (S/N 7560 & 7561)
AI 6	29	channel 6 (F/T SG5 HIGH S/N 7560)
AI 14	30	channel 6 (F/T SG5 HIGH S/N 7561)
AI 7	31	
AI 15	32	

* AI is analog input, PFI is programmable field interface

2.1.2 Motor Connections

Blocks 5-6-7 in Figure 6 show the motor connections. The aim was to control the stepper motor, which is a synchronous electric motor that can complete a full revolution in a large number of steps that result in linear movement. For this device, a stepper motor from Oriental Motors (DRL60MB4-05MG) was used because of its compact design and high positioning accuracy. They consist of a motor driver and an actuator and can

perform simple linear one-axis back and forth movement by following assumed calculations (DRL series user manual). The relationship between the displacement of the actuator (D), number of pulses (N) and resolution (R) is given by Equation (16). The relationship between the speed of the actuator (S), pulse rate (P) and resolution is given by Equation (17).

$$\mathbf{D=N\times R} \tag{16}$$

$$\mathbf{S=P\times R} \tag{17}$$

For controlling the motor the following hardware components were necessary.

- **NI PCI 7334 Motion Controller Card**: This is an integrated circuit (IC) chip specifically designed for controlling the motion of a stepping motor and the card was placed inside the PC in a vacant PCI slot.
- **Universal Motion Interface (NI UMI 7764)**: This is an interface that connects to the motion controller and the motor driver using a single connector. It outputs the pulse generated by the controller and makes the driver move the actuator. Table 3 shows the detailed wiring diagram of these motor connections.
- **Motor Driver**: The motor drivers are also ICs which were designed to drive the actuator of the motor, which is included with the stepper motor. They have three connectors which are connected to specific hardwares as shown in Table 3. The connector 1 was connected to the 24V power supply which controls the electromagnetic brake, connector 2 was connected to the NI UMI 7764 which controls pulse input, directional input and inhibitive output, and connector 3 was connected to the actuator.

Table 3: Pin diagram for motor connections

PIN ASSIGNMENTS	PURPOSE
	Driver connections
Power Supply	**Connector 1**
24V	elec/mag brake (red/white)
GND	(black/white)
Universal Motor Interface (UMI 7764)	
Motion Terminal Block	
Forward Limit	Limit swtich (blue colour)
Home Input	
Reverse Limit	Limit switch(white colour)
Inhibit Input	
Digital Ground	(green and black colour)
Analog Output	
Analog Output Ground	
	Connector 2
Inhibit Output	(black(brown))
Step(CW)	Pulse input (Black (red))
Dir(CCW)	Directional input (black(white))
5V(Output)	(red,white& brown)
Digital Ground	
	Connector 3
	(blue,red,orange,green and black motor lead to actuator)

2.2 LabVIEW Programing

Programming is the most crucial part of the Orthodontic wire tester and the selection of a programming platform was a critical decision because it would influence future device development. LabVIEW (Laboratory Virtual Instrumentation Engineering Workbench) is a platform and development environment for visual programming from National Instruments and is used to control different types of hardware. LabVIEW Version 7.1 platform was chosen to automate the orthodontic wire tester for three point bending test.

2.2.1 Sensor operations

It was very critical to understand the operating principles of the force/torque sensors from TWE (F/T transducer installation and operation manual (Document #9620-05-TWE-1)). Figure 7 shows the conceptual working of these sensors to determine the unloaded (reference measurement) and a loaded measurements. The unloaded measurement is used as a software biasing step to remove the effect of a constant load such as tooling weight. The difference of loaded and unloaded voltage values are multiplied with calibration matrix provided by the manufacturer to obtain force/torque values. Several programming steps are used to process the force and torque measurements.

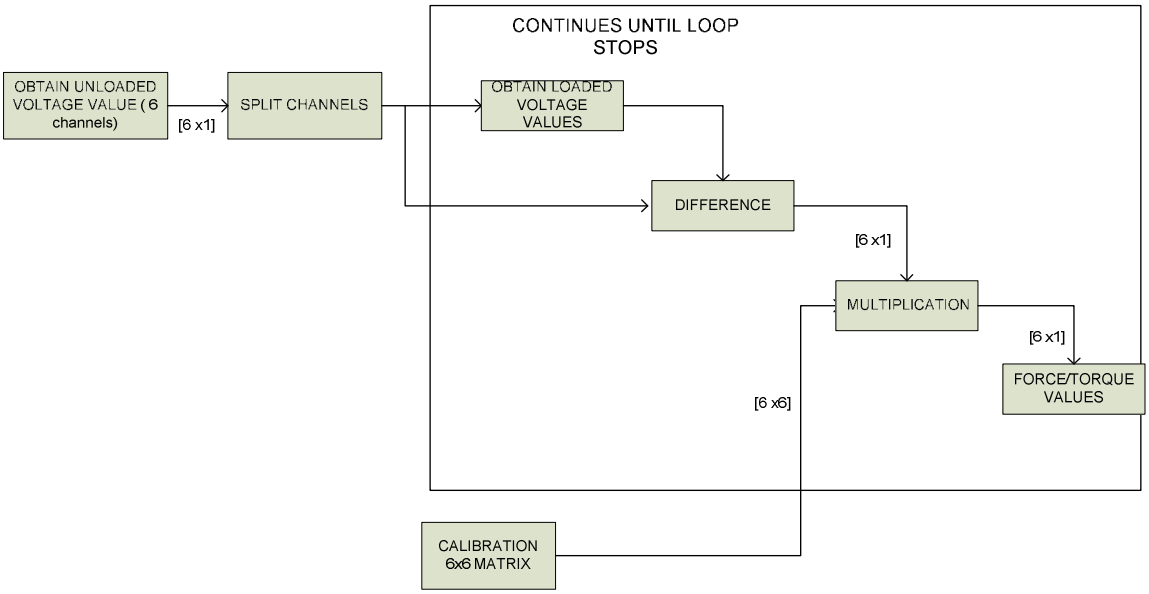

Figure 7: Flow chart of sensor measurement

The first step in programming these sensors was to get the raw voltage value from the sensor using the NI USB DAQ in LabVIEW. There were six channels from each sensor and LabVIEW was used to virtually configure each channels as shown in Figure

8. The voltage values, which are read from LabVIEW as an array of six values from both sensors, were split in order to analyze each channel individually.

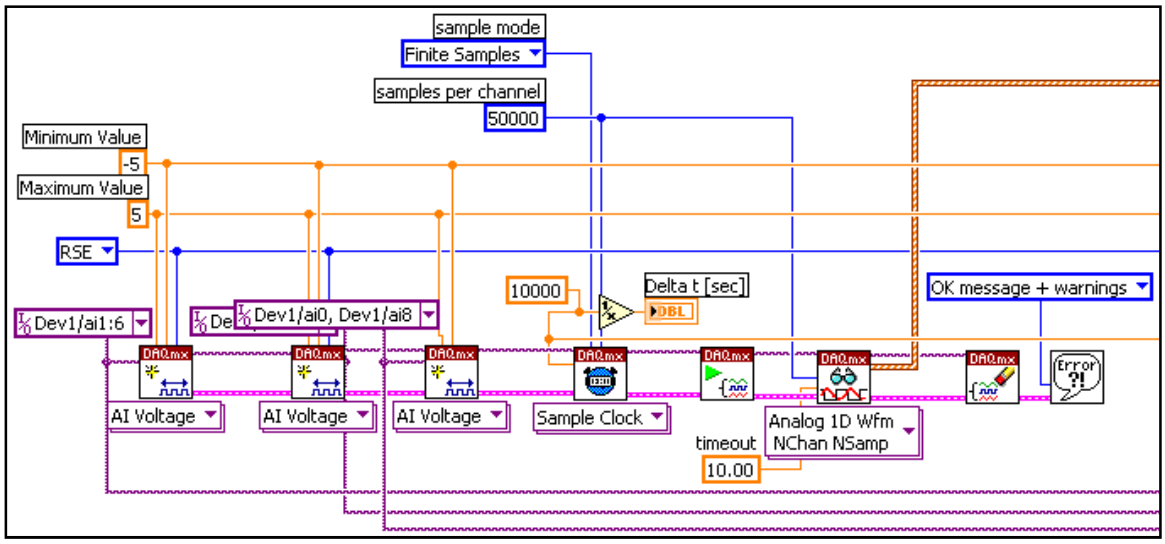

Figure 8: Block diagram of configuring sensors

A calibration matrix program was created as shown in Figure 9, to convert voltage values to force/torque values. The force/torque values are obtained by matrix multiplication using the change in voltage values for all six channels from the unloaded condition to the loaded condition and the [6 x 6] calibration matrix given by the sensor manufacturer.

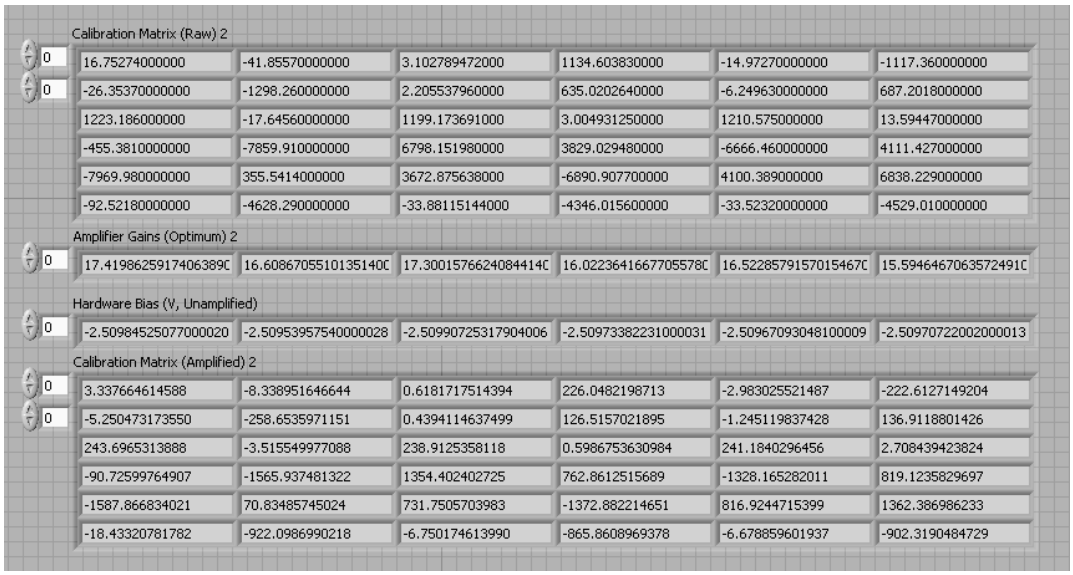

Figure 9: Front panel of calibration matrix program

A program to measure humidity and temperature measurement was also created. Each stage of the LabVIEW programming was tested and a final sensor measurement program which was capable of a continuous measurement of force/torque values, was developed by integrating all the subprogram routines. The front panel of sensor measurement program is shown in Figure 10.

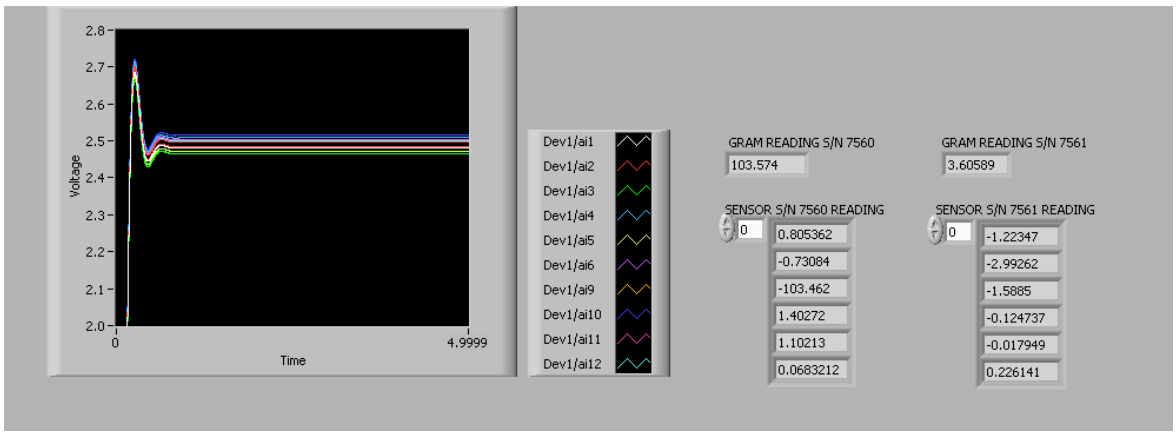

Figure 10: Front panel of sensor measurement program with IIR filter

2.2.1.1 Preliminary force/torque sensor verification

The following tests illustrated below were performed for developing an effective sensor measurement LabVIEW program by considering various factors including testing procedure, filter setting, sampling rate, and voltage regulation.

Individual axis testing

With the sensor at rest, voltage measurements of all six channels were taken and entered into the unloaded measurement area on the sample calculations worksheet. Figure 11 shows that known weights of 2g, 5g, 10g, 20g, 50g, 100g, 300g and 500g were placed in all the three axes individually over the surface of the sensor and measurements of all six channels were taken and entered into the loaded measurement area on the worksheet. Force/torque values were measured and recorded in grams (g) and gram millimeter (g-mm) respectively from the work sheet.

For performing this test, the following parameters were used: sampling rate of 10,000 Hz, 4 sec. measurement time for unloaded voltage values, and a 12V power supply was connected to the sensors.

A) **B)** **C)**

Figure 11: A) X axis testing , B) Y axis testing, C) Z axis testing

Filter testing

The performance of filter for seven different sampling rates (i.e., 10,000 Hz, 7,500 Hz, 5,000 Hz, 2,000 Hz, 1,000 Hz, 500 Hz and 250 Hz) were noted. In all the cases, the unloaded values were measured for 4 seconds and this process was repeated ten times. Mean and standard deviation of unloaded voltage values of all six channels were observed for both sensors with, and without, the LabVIEW IIR (Infinite Impulse Response) filter.

Sampling rate testing

An experiment was performed to optimize the sampling rate for force/torque measurements. Known weights of 5g, 10g, 50g, 100g and 500g respectively were placed over the Z axis (see Figure 11C) on both force sensors. Test conditions chosen were: four different sampling rates of 10,000 Hz, 5,000 Hz, 2,500 Hz and 1,500 Hz, 4 sec. measurement of unloaded voltage values, IIR filter of order 3 with cutoff frequency of 3 Hz, and a 12V power supply.

Torque testing

This test was performed to verify the torque values along the X axis by hanging the known weight of 50g at known distances of 0mm, 25mm, 50mm, 75mm, and 100mm, along the Z axis of both sensors as shown in Figure 12. The other parameters involved were a 1,500 Hz sampling rate, 12V power supply, and a IIR filter of order 3 and cutoff frequency of 3 Hz.

A) **B)**

Figure 12: A) Torque testing apparatus , B) free body diagram

2.2.1.2 Final force/torque sensor verification

The final verification was carried out after understanding all the key factors that were influencing the variability of sensor measurements. Initially, the 12V power supply was used for all the preliminary tests. Following the manufacturer's directions, it was changed to a 5V power supply. As three point bending test requires only Z axis measurement, the focus was on verifying the Z-axis performance of both sensors. Known weights of 10g, 20g, 50g, 100g, 200g and 500g were placed over the Z axis, as shown in Figure 13, and, for each weight, four trials were conducted.

The parameters used were a sampling rate of 10,000 Hz, a 4 sec. measurement of unloaded voltage values, an IIR filter of order 3 with cutoff frequency of 3Hz, force values measured continously for 5 seconds, and a 5V power supply.

Figure 13: Final Z axis verification

2.2.2 Motor operations

Motion controlling requires a clear understanding of the motion controller and the driver connections before programming. Initial motion verification was performed using the Measurement and Automation Explorer (MAX) software provided by NI. This is a software that allows for the testing of motor movement before creating the LabVIEW programs. Figure 14 shows the 1-dimentional interactive panel from the MAX software. The default settings of this software allows for the control of distance, speed, and a motion profile directly. It also has safety features like pause and continue and can kill the motion at any point of motor movement.

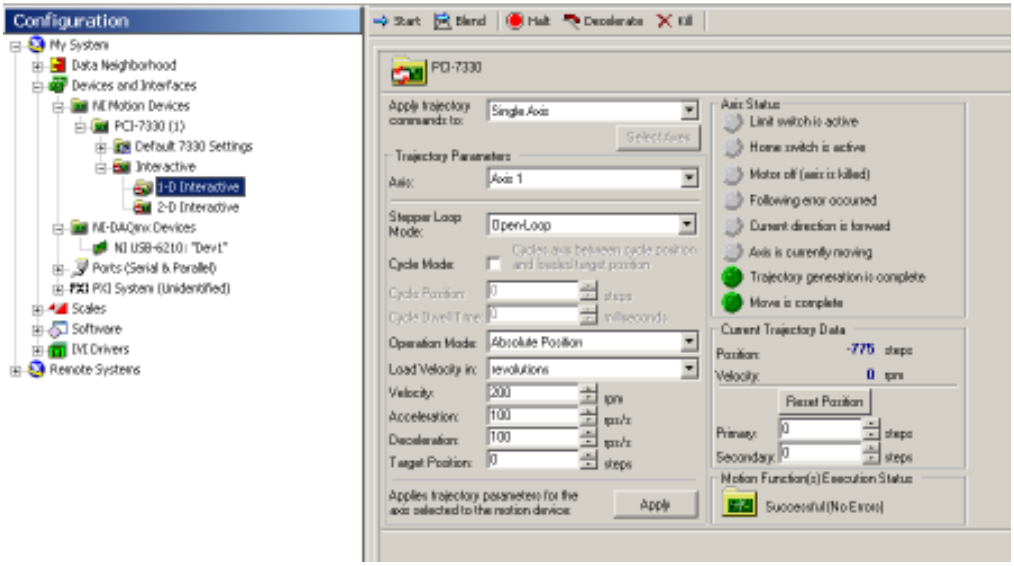

Figure 14: 1-dimentional interactive panel of measurement and automation explorer

The most important factor prior to programming was to have safety considerations of the device as motor can damage the sensors and other setup. A program was created to control the brake of the motor. Figure 15 shows the front panel of the brake control program.

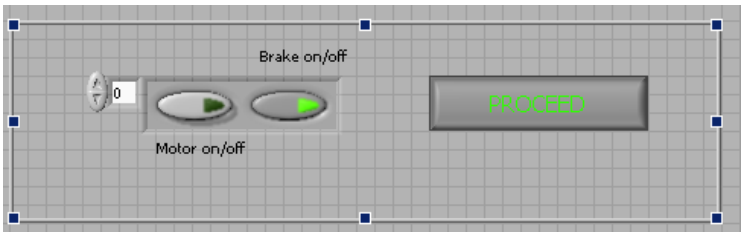

Figure 15: Front panel of Brake program

Similar to sensor measurement programming, it was required to create series of programs to control the motor completely with the first aspect of programming focused on initializing the motion controller. Figure 16 shows the flowchart of simple one-direction movement a separate program was created for back and forth movement of the actuator for specified distance & speed. The front panel of the program is shown in Figure 17.

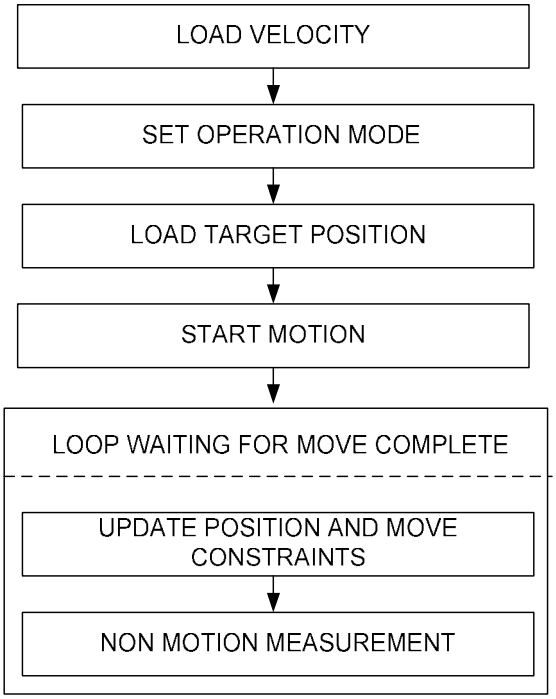

Figure 16: Flow chart of simple one-directional movement

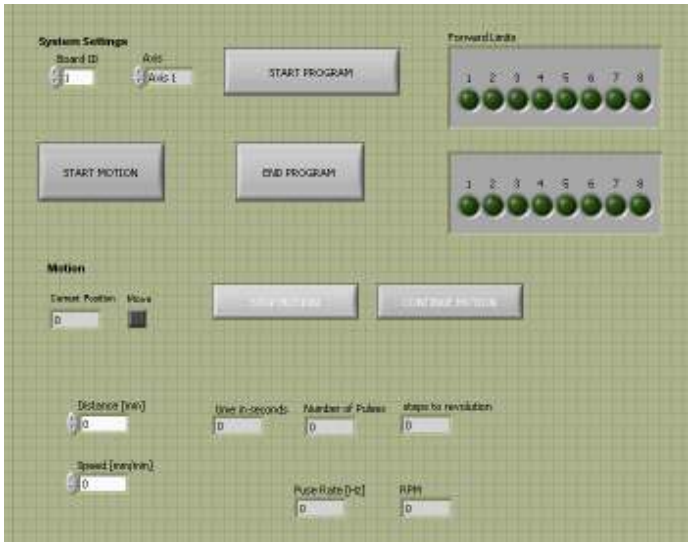

Figure 17: Front panel of the simple unidirectional movement

To implement the interrupt option to pause and continue the program in between the motor movement at any point of time, another program was developed. As the last programming step, a program was created by integrating all the program subroutines, which could perform all the operations discussed above.

2.2.2.1 Displacement Verification

The resolution of the motor was set at 0.004mm using a switch in the motor driver. The following motion profiles were tested for the distances: 1mm, 2mm, 3mm, 3.3mm, 3.5mm, 3.9mm, 5mm, and 10mm. Table 4 shows the test conditions of different motion profiles chosen for the displacement verification. Appendix A.1 details the direction sense of the motor.

Table 4: Motion profiles chosen for the displacement verification

Motion Profiles			
↓	↑	↓ ↑	↓ ↑ ↓

2.2.2.2 Velocity Verification

Table 5 shows the testing conditions under which the velocity of the motor was observed. This was done by observing the time the motor takes to reach the specified distance. Along with time, the number of pulses and the pulse rate were noted.

Table 5: Velocity verification test conditions

Test conditions			
Test #	Distance(mm)	Motion Profile	Velocity(mm/min)
1)	5	↓	0.5, 1, 2, 5, 7.5, 10, 15
2)	3	↑	0.5, 1, 2, 5, 7.5, 10, 15

2.3 Three Point bending test program

The crucial task was to incorporate the final sensor measurement program and the final motor program into one single program, which could perform the three point bending test. Since a feedback device was not incorporated correlation between the displacement and the force measurement was difficult. This required a series of programming attempts to create an effective three point bending test program as shown in Figure 18. Once the final program was created, various preliminary tests were performed with wood to verify the motor movement and sensor measurement simultaneously. There were two standard testing protocols followed for the three point bending test, as explained in Section 1.3.

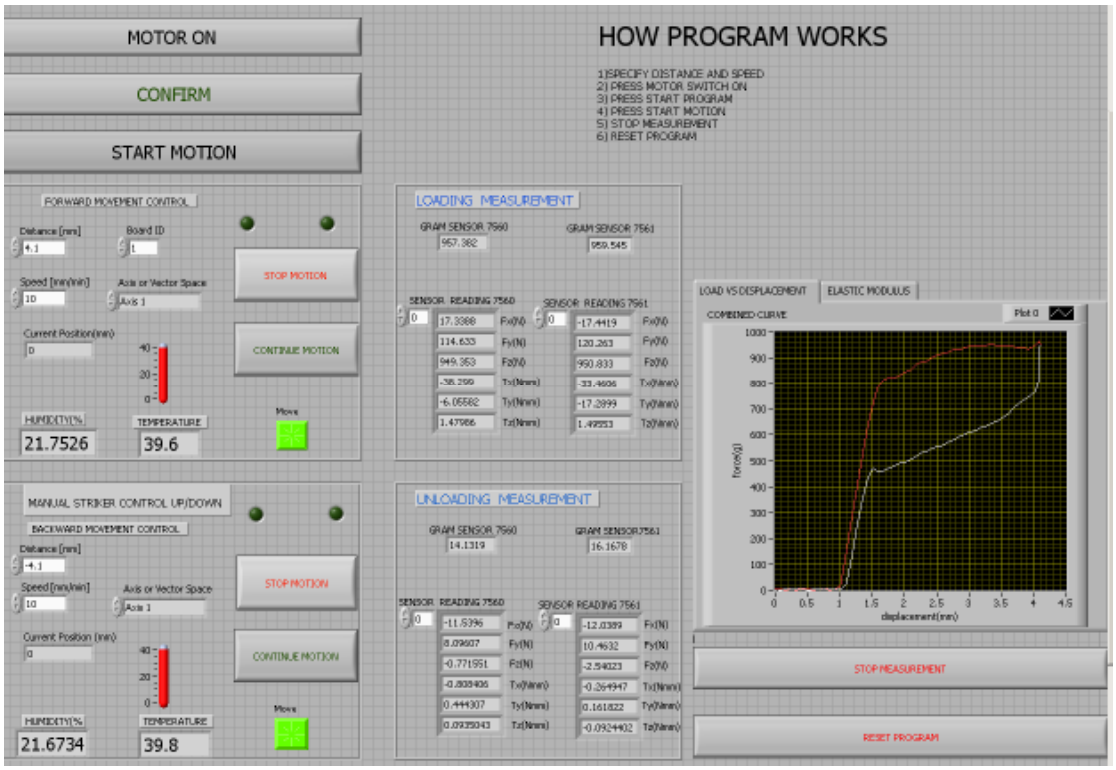

Figure 18: Front panel of the three point bending test program

2.3.1 ISO standard Testing

Test 1 - Old setting

The three point bending test was perfomed according to ISO standards on three round wires (0.012 inch, 0.014 inch and 0.016 inch) and three rectangular wires (0.016 x 0.022 inch, 0.018 x 0.025 inch, and 0.019 x 0.025 inch) of NiTi superelastic wire type, manufactured by Ortho Organizers (see Table 6). Figure 19A explains the wire placement location for this setting.

Table 6: List of NiTi wires tested using old setting

Wire Brand	Type	Round Wires(inch)	Rectangular Wires (inch)
Ortho Organizers	SE	0.012, 0.014,0.016	0.016 x 0.022, 0.018 x 0.025, 0.019 x 0.025

The following test conditions were applied in a 37° C environment:

1. The two posterior sections of the three archwires of the same batch were cut and tested.
2. A crosshead rate of striker was specified at 10mm/min, which provided a deflection of 3.1 mm (as shown in Table 1) .

The load/displacement curves were obtained for all the tests and the unloading forces were reported at different locations.

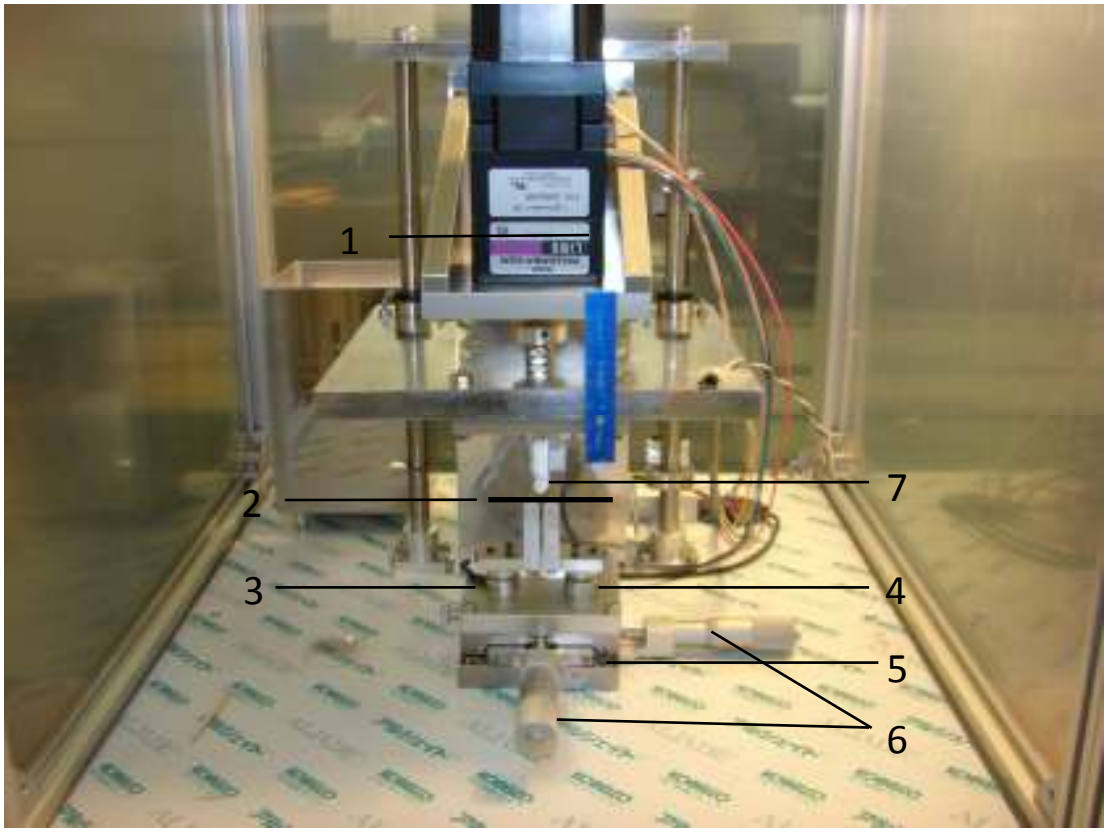

Figure 19A: Wire placement location of old setting

1. Motor
2. Specimen Wire
3. Left sensor (7560)
4. Right Sensor (7561)
5. XY Stage
6. Caliper.
7. Striker

Test 2 - New setting

The new setting used a striker and supports with a 60º angle and is shown in Figure 19B. All three point bending tests were performed as before (see Table 7). Also, a test was performed to examine the influence of crosshead rate on the load/displacement curves with the following test conditions:

1. Three samples of 0.016 inches and 0.016 x 0.022 wires.
2. Three different crosshead rates of the striker were used: 5mm/min, 7.5mm/min, and 10mm/min.

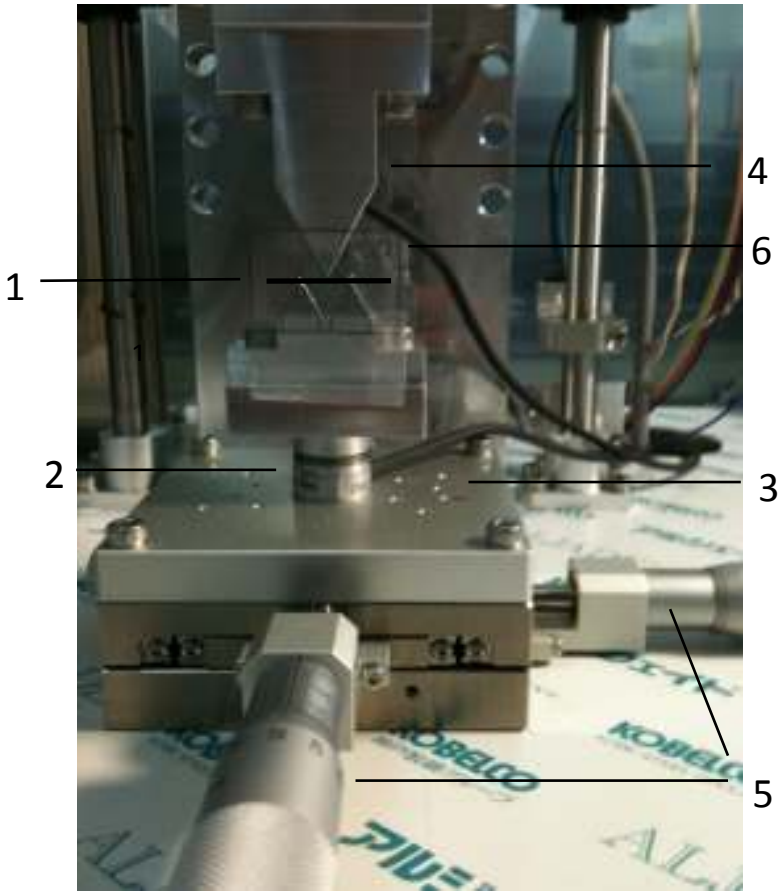

Figure 19B: New ISO setting

Table 7: List of NiTi wires tested using new setting

Wire Brand	Type	Round Wires(inch)	Rectangular Wires (inch)
Ortho Organizers	SE	0.012, 0.014,0.016	0.016 x 0.022, 0.018 x 0.025, 0.019 x 0.025
Ultimate Wireforms	SE	0.012	0.016 x 0.022

2.3.2 ANSI standard Testing

The testing protocol for the ANSI standard was slightly different from the ISO standard in regards to the testing setup. The ISO setting was changed to an ANSI setting (see Appendix A.1) and the three point bending test was performed for the same set of wires tested under the ISO standard.

The following test conditions were applied in a 37° C environment:

1. Six samples with specimen length of 50mm specimen for each size of wires was taken.
2. Similar to ISO (as explained in section 2.3.1), at crosshead rate of the striker was maintained at 10mm/min, which provided a deflection of 3.1 mm.

2.4 Jacobian matrix derivation

As explained in Section 1.5 the Jacobian matrix was derived using the translation and rotation of the coordinate systems.

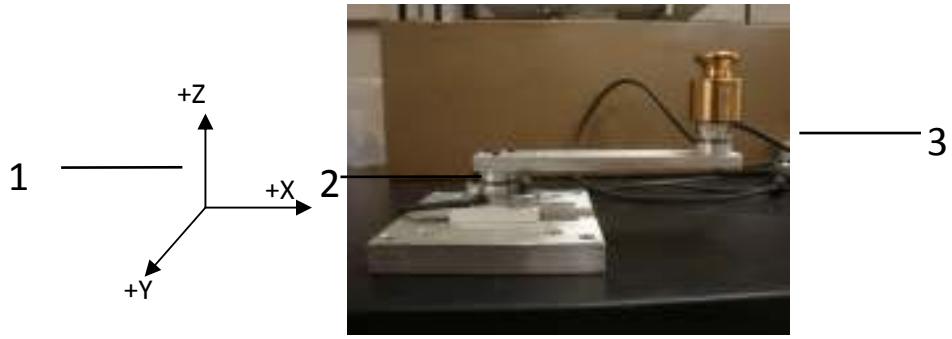

Figure 20: Preliminary Jacobian setting

1. Co ordinate system of Sensor S/ N 7560
2. Sensor S/N 7560
3. Sensor S/N 7561

Figure 20 illustrates the testing setup. A sensor with S/N 7560 was mounted at the bottom of the aluminum plate of length 100mm and the sensor with S/N 7561 was mounted at the top. The sensor 7561 was rotated and translated over the plate with respect to sensor 7560 to create multiple test conditions. The coordinate system of 7560 is indicated in Figure 20 and the center of the top surface of the sensor was considered as the origin.

Table 8: Various testing conditions for placing sensor 7561with respect to sensor 7561

TEST CONDITIONS			
	X axis	Y axis	Z axis
ROTATION(degrees)	0	180	30,60,90
TRANSLATION(mm)	100,50,25	0	0

As shown in Table 8, a known rotation and translation was chosen for sensor 7561. From the equations discussed in the Section 1.4, a Jacobian matrix was derived for each of the testing conditions. The known weights were placed over sensor 7561 and the values obtained from both sensors were noted. Equations (18) and (19) show the force/torque values from the sensors. The force/torque values which were measured using sensor 7561 is equivalent to the matrix multiplication of [6x6] Jacobian matrix and the force/torque values from sensor 7560, as demonstrated in Equation (20) which shows the Jacobian transformation.

Various experiments were performed using the conditions given in Table 8 and the set up shown in Figure 20 to test Equation (20) for its validity. It was determined that this setup was not able to validate Equation (20), so a new method was developed and is presented in section 2.4.1.

$$\mathbf{F}_{7561} = [f_x \quad f_y \quad f_z \quad t_x \quad t_y \quad t_z]^T \tag{18}$$

$$\mathbf{F}_{7560} = [f_{x1} \quad f_{y1} \quad f_{z1} \quad t_{x1} \quad t_{y1} \quad t_{z1}]^T \tag{19}$$

$$\begin{bmatrix} f_x \\ f_y \\ f_z \\ t_X \\ t_y \\ t_z \end{bmatrix} = \mathbf{J} \times \begin{bmatrix} f_{x1} \\ f_{y1} \\ f_{z1} \\ t_{X1} \\ t_{y1} \\ t_{z1} \end{bmatrix} \tag{20}$$

2.4.1 Final Jacobian validation

Setup 1 – Only translation

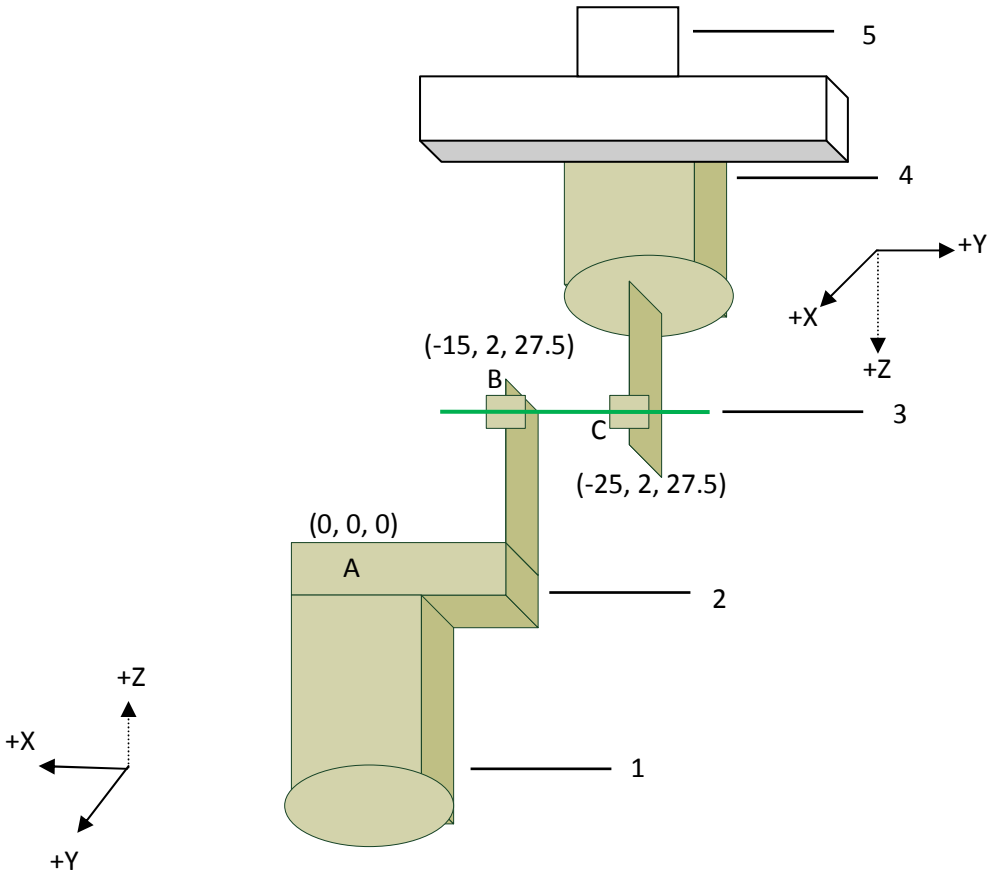

Figure 21: Final testing setup of Jacobian validation for left tooth

1) Sensor S/N 7560
2) Aluminum plate
3) Orthodontic arch wire
4) Sensor S/N 7561
5) Motor

Figure 21 illustrates the final testing setup for the Jacobian matrix and assumed that the whole setup was a perfect rigid body. Sensor 7560 was mounted at location A, which is the origin (0, 0, 0) coordinate while the sensor 7561 was mounted at the top and attached to the motor. Points B and C in Figure 21 were chosen as exact tooth locations for a 0.021 x 0.025 inch NiTi and straight beta CNA archwire attached to a 0.025 inch bracket. The coordinates of point B with respect to sensor 7560 is (-15, 2, 27.5) and the coordinates of point C is (-25, 2, 27.5) with respect to the same sensor.

In this testing, the motor moves 2mm in forward direction and generates a known force at point C. This applied force/torque values were measured using sensor 7561 and the received force/torque values were measured using sensor 7560. In order to measure force/torque exactly at the point B, a 6x6 Jacobian matrix was derived using a the 4x4 transformation matrix. The transformation matrix, **H,** due to the translation of the vector (-15, 2, 27.5) is given by Equation (21).

$$\mathbf{H}=\begin{bmatrix}\mathbf{1} & \mathbf{0} & \mathbf{0} & \mathbf{-15}\\ \mathbf{0} & \mathbf{1} & \mathbf{0} & \mathbf{2}\\ \mathbf{0} & \mathbf{0} & \mathbf{1} & \mathbf{27.5}\\ \mathbf{0} & \mathbf{0} & \mathbf{0} & \mathbf{0}\end{bmatrix} \tag{21}$$

$$\mathbf{n=1\ i+0\ j+0\ k} \tag{22}$$

$$\mathbf{o=0\ i+1\ j+0\ k} \tag{23}$$

$$\mathbf{a=0\ i+0\ j+1\ k} \tag{24}$$

$$\mathbf{p=-15\ i+2\ j+27.5\ k} \tag{25}$$

where, **n**, **o**, **a** and **p** are column vectors of the transformation matrix and are given by Equations (22), (23), (24) and (25) respectively. Substituting these values in Equation (8), the Jacobian matrix, **J**, was obtained from the translation as shown in Equation (26).

$$J=\begin{bmatrix} 1 & 0 & 0 & 0 & 0 & 0 \\ 0 & 1 & 0 & 0 & 0 & 0 \\ 0 & 0 & 1 & 0 & 0 & 0 \\ 0 & -27.5 & 2 & 1 & 0 & 0 \\ -27.5 & 0 & -15 & 0 & 1 & 0 \\ 2 & -15 & 0 & 0 & 0 & 1 \end{bmatrix} \quad (26)$$

The force/torque at point B is given by Equation (27).

$$Fb=[f_{bx} \quad f_{by} \quad f_{bz} \quad t_{bx} \quad t_{by} \quad t_{bz}]^T = J \times F_{7560} \quad (27)$$

Since it is a rigid body system, the applied force should be equal to the received force as shown in Equation (28).

$$F_{7560}=F_{7561} \quad (28)$$

At point B, the force applied is predominantly in Z direction but the torque along the Y axis was observed with the change in displacement. Theoretically, the torque along the Y axis can be calculated using the Equation (29).

$$t_{by}=10 \times F_z \quad (29)$$

where F_z is the applied force along Z-axis measured by sensor 7561. The expected torque was then compared with observed torque at point B.

Setup 2 - Rotation & translation

Because setup 1 did not consider any rotational movement, a new setup was designed to verify the Jacobian matrix involving both rotational and translational movements. As illustrated in Figure 22, set up 2 is symmetrical to set up 1 in the right-hand side but sensor 7560 was rotated 60 degrees along the Z axis. In order to measure the force/torque value at point B, the Jacobian matrix had to be derived again. The

transformation matrix, due to rotation and translation, is given by H, as shown in Equation (30).

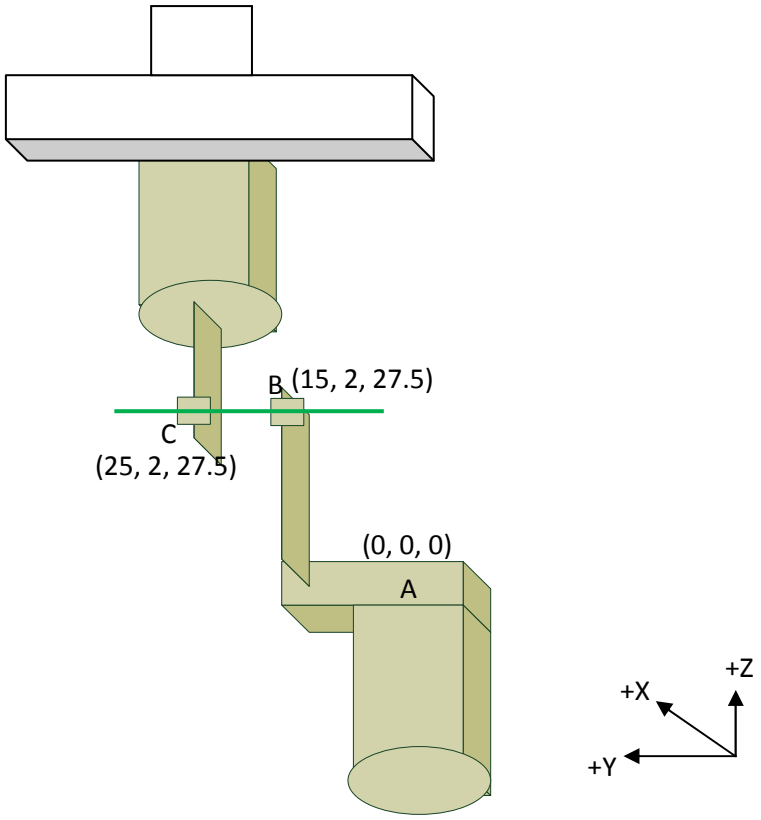

Figure 22: Testing setup of Jacobian validation with rotation

$$\mathbf{H=rot\ (z,\ 60)\times trans(15,2,27.5)} \tag{30}$$

The Jacobian matrix derived from this transformation matrix is given by Equation (31)

$$\mathbf{J}=\begin{bmatrix} \cos\theta & \sin\theta & 0 & 0 & 0 & 0 \\ -\sin\theta & \cos\theta & 0 & 0 & 0 & 0 \\ 0 & 0 & 1 & 0 & 0 & 0 \\ -27.5\sin\theta & -27.5\cos\theta & 2 & \cos\theta & \sin\theta & 0 \\ 27.5\cos\theta & -27.5\sin\theta & -15 & -\sin\theta & \cos\theta & 0 \\ 15\sin\theta-2\cos\theta & 15\cos\theta+2\sin\theta & 0 & 0 & 0 & 1 \end{bmatrix} \tag{31}$$

θ=60 degree

As with the case of previous setup, Equations (27), (28), and (29) still hold the same and expected torque value at point B as compared with the observed torque.

3 Results

3.1 Preliminary force/torque sensor program verification

3.1.1 Individual axis load application

For preliminary testing, known weights were applied to the individual axis (see Figure 4), of the sensors according to the axis of interest. The voltage values before and after the application of load, referred as unloaded and loaded measurements, were noted down for all six channels for five trials as shown in Table 9. Channel 1(ch.1) through channel 6 (ch.6) are the voltage values of the all the channels of sensor 7560. The force values along the X (Fx[N]), Y (Fy[N]) and Z (Fz[N]) axes, in Newtons, and the torque values along the X (Tx[Nmm]), Y (Ty[Nmm]) and Z (Tz[Nmm]) axes, in Newton millimeters are presented in Table 9. The summation of force values in Newtons (Sum F[N]) and grams (Sum F[g]) are also provided in Table 9. The difference between the loaded measurement and the unloaded measurement values were multiplied to the calibration matrix to get the force and torque values. As indicated in Table 9, a 100g load was applied over the Y-axis of sensor 7560. It was observed that Channel 3 had the lowest mean unloaded voltage value of 6.717976 volts and Channel 4 had the highest value of 6.8400038 volts. The standard deviation ranged from 0.001771 to 0.00536 volts and the mean loaded voltage value ranged from 6.703902 to 6.843846 volts.

All the loaded and unloaded measurement values were entered in the sample calculation sheet provided by the manufacturer and force/torque values were noted down manually for all the trials. A variability was observed in the Sum F[g] values with the lowest being 92.32g and the highest being 137.6g. Since the load was applied over Y axis, the Y-component of force (i.e., Fy[N]) changed from .8933 to 1.1556 N. It was

observed that the torque along X axis (Tx[Nmm]) changed for each trial. The variability in these measurements were analyzed extensively and the error associated was minimized through testing and results of which are presented in the following sections.

Table 9: 100g load applied on Y axis over sensor S/N 7560

Sensor I - S/N FT7560							
100g							
	Unloaded [V]						
	Trial #1	Trial #2	Trial #3	Trial #4	Trial #5	Average	St.Dev.
Ch.1	6.78221	6.78801	6.78818	6.78537	6.78850	6.78645	0.00268
Ch.2	6.83051	6.83348	6.83513	6.83209	6.83387	6.83302	0.00177
Ch.3	6.71649	6.71994	6.72056	6.71795	6.71495	6.71798	0.00234
Ch.4	6.83865	6.84399	6.84468	6.84144	6.83144	6.84004	0.00536
Ch.5	6.76282	6.76999	6.77066	6.76610	6.75781	6.76547	0.00533
Ch.6	6.81994	6.82674	6.82772	6.82417	6.82010	6.82373	0.00363
	Loaded [V]						
	Trial #1	Trial #2	Trial #3	Trial #4	Trial #5	Average	St.Dev.
Ch.1	6.78316	6.79076	6.78960	6.78655	6.78710	6.78743	0.00296
Ch.2	6.82064	6.82561	6.82621	6.82330	6.82363	6.82388	0.00220
Ch.3	6.70094	6.70526	6.70896	6.70490	6.69945	6.70390	0.00378
Ch.4	6.84239	6.84822	6.84728	6.84355	6.83779	6.84385	0.00418
Ch.5	6.77773	6.78805	6.78188	6.77931	6.77390	6.78017	0.00527
Ch.6	6.82400	6.82964	6.83029	6.82571	6.82524	6.82698	0.00281
	Calculated						
	Trial #1	Trial #2	Trial #3	Trial #4	Trial #5	Average	St.Dev.
Fx [N]	-0.14469	-0.03943	-0.08823	-0.06127	-0.04789	-0.07630	0.04246
Fy [N]	1.15561	0.96172	0.96662	0.89335	1.35029	1.06552	0.18669
Fz [N]	0.06052	0.54289	0.11457	0.14339	-0.03372	0.16553	0.22148
Tx [N-mm]	-6.95901	-9.20762	-4.60058	-6.65269	-6.29918	-6.74382	1.65198
Ty [N-mm]	-0.03855	-0.56976	-0.50807	-0.41135	0.92882	-0.11978	0.62137
Tz [N-mm]	0.39764	-0.09486	0.97445	1.37491	-0.61747	0.40693	0.80005
Sum F [N]	**1.16620**	**1.10507**	**0.97738**	**0.90686**	**1.35156**	**1.10142**	**0.17322**
Sum F [g]	**118.87895**	**112.76226**	**99.73255**	**92.53672**	**137.91466**	**110.73655**	**19.95892**

3.1.2 Sampling rate optimization

A known 50g weight was placed over the Z-axis. The effect of the force values at different sampling rates were compared, as shown in Table 10 and 11. Force and torque values (Fx, Fy,Fz,Tx,Ty,Tz) were measured in Newtons and Newton millimeters for each axis and the force value along the Z axis is given as Sum Fz[g] in grams in Tables 10 and 11. For each sampling rate, 10 trials were performed and the mean and standard deviation were recorded. It was observed that the mean and standard deviation values for 50g weight at 10,000Hz was 50.18g and 0.39339 for sensor 7560. For sensor 7561, the mean and standard deviation values were 50.03g and 0.02081g. A t-test with a 95% confidence interval for all the mean values revealed that there were no significant differences with the changing of the sampling rates. It was also observed that the error in the force measurement decreased appreciably.

Table 10: Comparing 50g weight at different sampling rate over Z axis of sensor S/N 7560

Sensor I - S/N FT7560								
50g								
	SAMPLING RATE(Hz)							
	10000.00000		5000.00000		2500.00000		1500.00000	
	Average	St.Dev.	Average	St.Dev.	Average	St.Dev.	Average	St.Dev.
Fx [N]	0.00012	0.00203	0.00334	0.00203	0.00545	0.00211	0.00363	0.00192
Fy [N]	0.00457	0.00089	0.00506	0.00008	0.00346	0.00155	0.00463	0.00305
Fz [N]	0.49230	0.00386	0.50194	0.00463	0.49564	0.00849	0.49401	0.00542
Tx [N-mm]	1.60323	0.30121	1.25083	0.32683	1.13524	0.52287	-1.54025	0.21692
Ty [N-mm]	0.20012	0.21146	0.28083	0.27960	0.26607	0.50276	0.21972	0.22669
Tz [N-mm]	0.02170	0.00212	0.03718	0.01790	0.00161	0.03854	0.01163	0.02287
SUM Fz[g]	**50.18359**	**0.39339**	**51.04529**	**0.47237**	**50.52413**	**0.86490**	**50.35810**	**0.55204**

Table 11: Comparing 50g weight at different sampling rate over Z axis of sensor S/N 7561

Sensor 2 - S/N FT7561								
50g								
	SAMPLING RATE(Hz)							
	10000.00000		5000.00000		2500.00000		1500.00000	
	Average	St.Dev.	Average	St.Dev.	Average	St.Dev.	Average	St.Dev.
Fx [N]	0.00754	0.00725	-0.00838	0.00725	-0.00880	0.00211	-0.00635	0.00451
Fy [N]	0.00308	0.00005	0.00312	0.00005	0.00246	0.00065	0.00406	0.00702
Fz [N]	0.49102	0.00204	0.50367	0.00463	0.49978	0.00449	0.49399	0.00577
Tx [N-mm]	1.75382	0.15646	1.84956	0.31048	1.11112	0.58602	-1.40002	0.20002
Ty [N-mm]	0.21237	0.21211	0.28899	0.25645	0.26112	0.52346	-0.21235	0.59875
Tz [N-mm]	0.03718	0.01002	0.03191	0.01112	0.00345	0.03331	0.00237	0.03854
SUM Fz[g]	**50.03524**	**0.20810**	**51.11129**	**0.40955**	**50.94567**	**0.48473**	**50.35540**	**0.58837**

3.1.3 Torque testing

As shown in Figure 12, this test examined the torque values along the X-axis of both the sensors. In Tables 12 and 13, 50g known weight was hung around the Z-axis at various distances along the Y axis of the sensors. Tx, Ty, Tz were the torque values which were measured in Newton millimeters along the X, Y and Z axes. The torque values were then compared with the theoretical values, which is given by Equation (32).

$$\tau = Dy \times Fz \tag{32}$$

The mean and standard deviation of torque values were also recorded for the 5 trials. When the 50g was hung at 0 mm, 25mm, 50mm, 75mm, and 100mm, the product of distance times the force was very close to the expected value and had small percentage error of only 0.04%.

Table 12: Hanging 50g weight around Z axis at known distances of sensor S/N 7560

Sensor I - S/N FT7560						
50g						
distance(mm)						
	Tx[Nmm]		Ty[Nmm]		Tz[Nmm]	
	Average	St.Dev.	Average	St.Dev.	Average	St.Dev.
0.00000	0.18160	0.00120	0.35450	0.00100	-0.02181	0.00200
25.00000	-12.01150	0.01220	0.48015	0.02100	-0.21596	0.07800
50.00000	-24.50240	0.00330	0.97120	0.01400	-0.42818	0.05400
75.00000	-36.46420	0.00100	-0.23940	0.00200	-0.57692	0.00600
100.00000	-49.48570	0.02210	0.37940	0.09100	-0.78781	0.02300

Table 13: Hanging 50g weight around Z-axis at known distances of sensor S/N 7561

Sensor 2 - S/N FT7561						
50g						
distance(mm)						
	Tx[Nmm]		Ty[Nmm]		Tz[Nmm]	
	Average	St.Dev.	Average	St.Dev.	Average	St.Dev.
0.00000	0.13130	0.00210	0.51230	0.00300	0.03410	0.00100
25.00000	-12.00320	0.03120	0.43221	0.03000	-0.04320	0.00540
50.00000	-24.00040	0.01100	0.87777	0.05600	0.32120	0.02000
75.00000	-36.41140	0.00200	0.34112	0.53000	0.34440	0.01110
100.00000	-48.99860	0.03230	0.12320	0.06700	-0.63420	0.04120

3.2 Final Force/Torque sensor program verification

Tables 14 and 15 shows that different loads applied over the Z axis of both the sensors and Fx, Fy, and Fz were the force values on X, Y and Z axis, measured in grams, respectively. For the weights lesser than 50g, the percent error was found to be 5%. The average percent error for weights from 50g to 500g was calculated to be 0.5%. The percent error was calculated by the Equation (33), where the expected values were the known weights and observed results were the actual values.

$$\% \text{ Error} = \frac{\text{Actualvalue-Expected value}}{\text{Expected value}} * 100 \qquad (33)$$

Table 14: Load applied along Z-axis of sensor S/N 7560

Sensor I - S/N FT7560						
Weights(g)						
	Fx[g]		Fy[g]		Fz[g]	
	Average	St.Dev.	Average	St.Dev.	Average	St.Dev.
10.00000	-0.09409	0.20206	-0.21445	0.15771	10.57491	0.49084
20.00000	0.18209	0.18990	-0.55736	0.08601	20.95227	0.37865
50.00000	-0.33655	0.17668	-0.47700	0.13830	50.36455	0.35949
100.00000	-0.77891	0.09044	-0.31973	0.19940	100.51130	0.28857
200.00000	-0.99727	0.18101	-1.15391	0.15228	201.26250	0.47287
500.00000	-2.39427	0.18753	-3.48045	0.14200	502.05000	0.17732

Table 15: Load applied along Z-axis of sensor S/N 7561

Sensor 2 - S/N FT7561						
Weights(g)						
	Fx[g]		Fy[g]		Fz[g]	
	Average	St.Dev.	Average	St.Dev.	Average	St.Dev.
10.00000	1.17382	0.17984	0.05709	0.21153	9.83536	0.26655
20.00000	-0.66373	0.18681	0.32427	0.17522	20.27864	0.27092
50.00000	-0.00091	0.12383	0.54155	0.14204	50.82818	0.28397
100.00000	0.80709	0.32721	1.00346	0.17389	100.52250	0.45242
200.00000	1.72864	0.24994	1.91200	0.08700	201.28870	0.50718
500.00000	3.65882	0.16892	4.69000	0.08892	502.30000	0.47659

3.3 Displacement & Velocity verification

Table 16: Velocity verification by comparing average expected time vs. actual time of 5mm distance

	Velocity(mm/min)	Velocity(rpm)	Pulse rate (Hz)	Number of Pulses	Actual Time taken (sec)	Expected time(sec)
1)	0.500	0.125	2.083	1250.000	591.000	600.000
2)	1.000	0.250	4.167	1250.000	295.000	300.000
3)	2.000	0.500	8.333	1250.000	148.200	150.000
4)	5.000	1.250	20.833	1250.000	60.200	60.000
5)	7.500	1.825	31.250	1250.000	40.320	40.000
6)	10.000	2.500	41.667	1250.000	30.160	30.000
7)	15.000	3.750	63.500	1250.000	20.400	20.000

For all the motion profiles, the displacements mentioned in section 2.2.2.1 were verified using a finely graduated ruler. As demonstrated in Table 16, different velocities were tested at a known distance of 5mm and the time, the number of pulses, and, the pulse rate were recorded. All the values matched the theoretical calculations but it was

observed that the error increased with decreasing velocity. The predicted time for moving 5mm at 0.5mm/min was 600 seconds but the actual time it took to reach this distance was 591seconds. Using Equation (24), the error associated with a velocity of 0.5mm/min was calculated to be 1.5%. The average error for the other velocities was less than 0.05%, which were considered negligible for this application.

3.4 Three point bending test

3.4.1 Old setting ISO Results

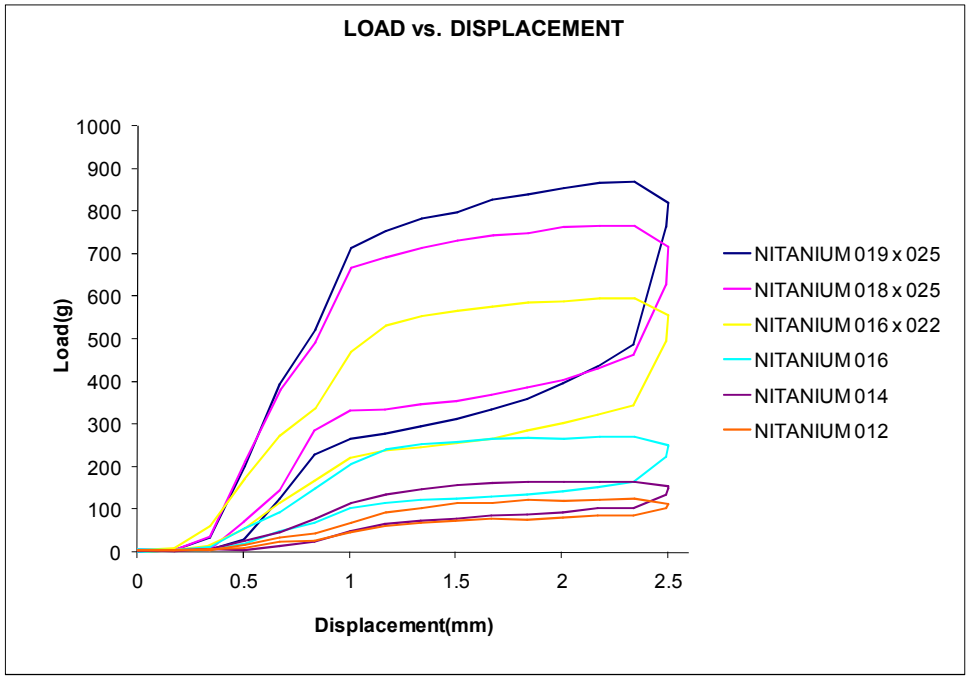

Figure 23: Comparison of Load/Displacement curves of six different sizes of Ni Ti

Figure 23 demonstrates the load displacement curves of six varying sizes of Ortho Organizers Super Elastic NiTi wires. The ISO testing protocol requires loading the wire up to 3.1mm and returning back to 0 mm but, due to design flaws, it was decided to push only to a limit of 2.5mm and the back to 0 mm. It was clearly observed that, when the striker was about to reach 2.4mm, there was an obvious downward slope in the loading

curves. All the wires showed similar patterns because of the sliding these wires experienced the surface of the support. It was observed that by changing the size of the wire, the loading/unloading profile changed drastically as well. As indicated in Table 17, the 0.019 x 0.022 rectangular wires had the maximum average peak force of 820.5g with a standard deviation of 10.03g. The 0.012 inch round wire had the least average peak force of 113.43g with a standard deviation of 1.22g. The super elastic property of the wires was not properly shown with this setting. This necessitated the need for a change in the testing set up in order to properly perform the ISO standard testing.

Table 17: Old setting unloading forces for different wire sizes

	Unloading forces (g) at different locations (mm)							
	2.50000		1.50000		1.00000		0.50000	
Wire size(in)	Mean	Std	Mean	Std	Mean	Std	Mean	Std
019 x 025	820.50000	10.03000	311.80000	8.23000	266.90000	6.21000	28.76000	2.57000
018 x 025	716.20000	9.11000	355.89000	8.99000	332.81000	7.20000	70.90000	4.20000
016 x 022	557.00000	8.20000	256.30000	4.23000	222.60000	3.25000	53.40000	2.90000
16.00000	249.82000	4.22000	126.11000	5.32000	104.46000	3.45000	18.90000	1.78000
14.00000	151.03000	3.45000	79.46000	2.11000	50.37100	1.11000	4.88000	0.45000
12.00000	113.43000	1.22000	74.44000	1.24000	45.94000	1.40000	9.34000	2.10000

3.4.2 New ISO setting result

The actual ISO testing protocols were followed with this setting. All the wires were tested in the temperature range of 36 ± 1 degree celsius and each wire was subjected to the symmetrical three point bending test. The striker was placed exactly 1 mm above the specimen wire and the wire was deflected to 3.1 mm at a cross head speed of 10mm/min from the point of contact with the striker. Figures 23 and 24 illustrates the load/displacement curves of 3 brands of rectangular wires (0.016 x 0.022, 0.018 x 0.025, 0.019 x 0.025) and 3 brands round wires (0.012, 0.014, 0.016) from Ortho Organizers. It was noted that the force values were nearly zero in the region of 0 to 1 mm displacement.

After 1mm, the force values were observed to linearly until it reached its elastic limit at 1.6mm.

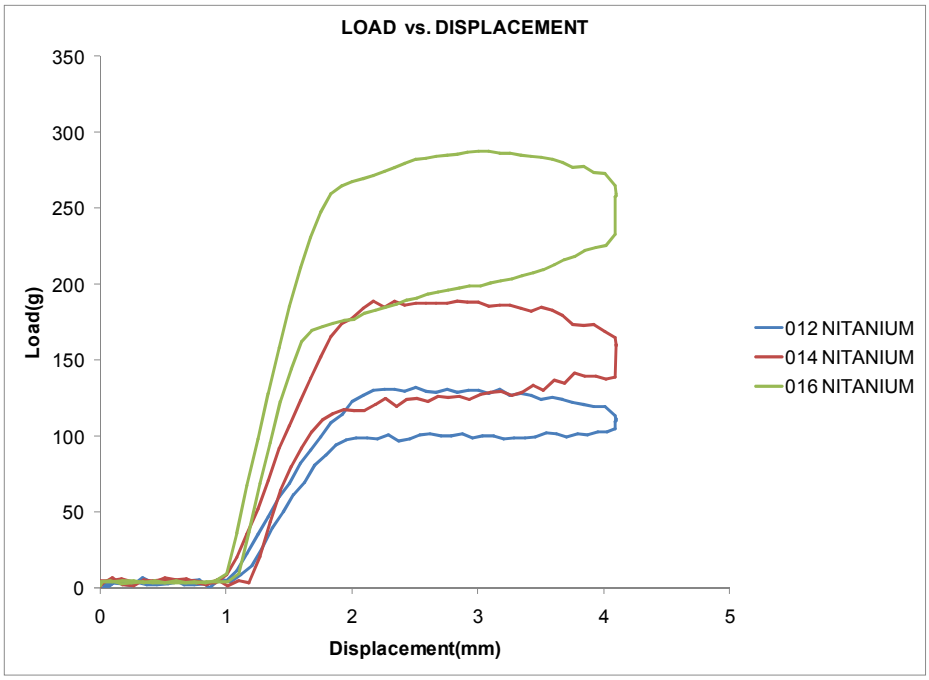

Figure 24: Comparison of load/ displacement Curves of 3 Rectangular wires

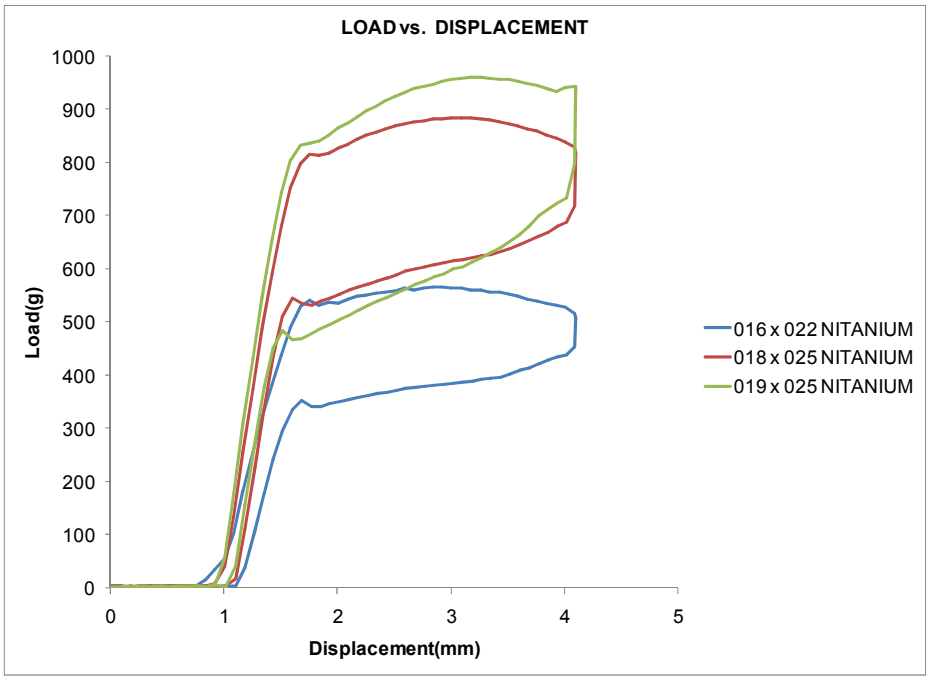

Figure 25: Comparison of load/displacement Curves of 3 round wires

Table 18: Unloading bending forces at 4 different locations for 6 different sizes of ortho organizers in ISO setting

	Unloading forces (g) at different locations (mm)							
	3.00000		2.00000		1.00000		0.50000	
Wire size(in)	Mean	Std	Mean	Std	Mean	Std	Mean	Std
019 x 025	734.66609	32.12300	600.36594	21.80117	504.65213	8.56725	484.64813	4.21190
018 x 025	687.63324	22.03465	615.91788	16.81804	552.63751	15.85544	510.34000	10.03440
016 x 022	438.21591	3.46708	385.99064	3.98465	351.07528	4.64601	295.69201	3.94857
16.00000	225.88000	4.08707	199.20840	3.00564	177.15914	2.11340	144.34407	1.32560
14.00000	141.09467	3.00230	128.59047	2.87460	116.24409	2.11340	68.83454	1.25470
12.00000	102.84085	1.84840	100.13085	0.40432	98.84333	0.41111	61.33450	0.53478

The bending force during the unloading process was determined from this load/displacement curves and is reported in Table 18. The 0.019 x 0.025 had the maximum force of 734.666g at 3mm with standard deviation of 32.123g and the 0.012 inch wire had the minimum peak force of 102.8409g at 3mm.

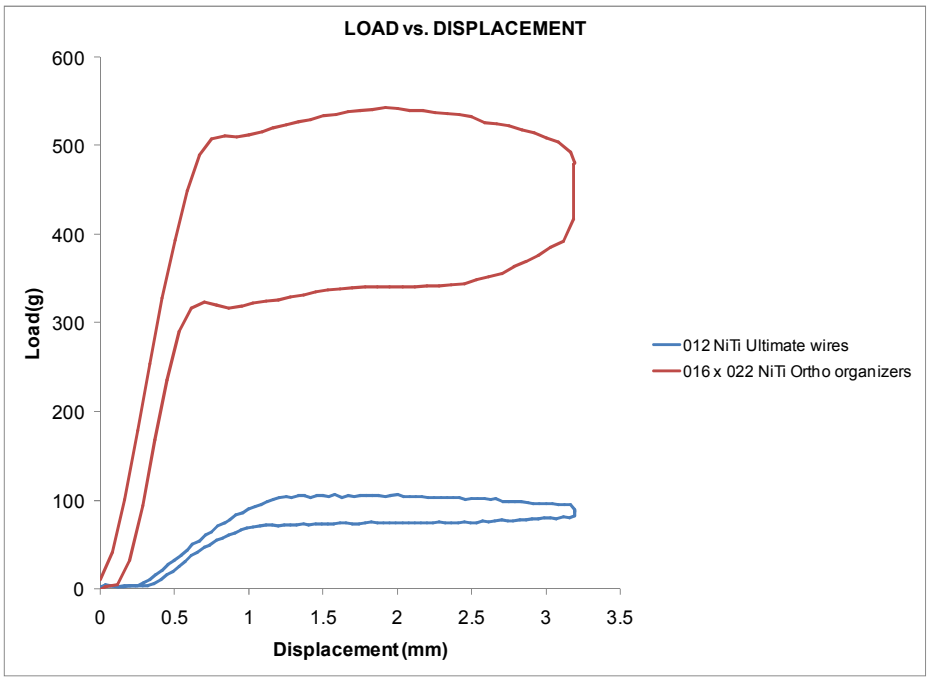

Figure 26: Comparison of load/displacement curves of rectangular 0.016 x 0.022 and 0.012 round ultimate wires

Figure 26 shows load/displacement curves of 0.012 inch round wire and 0.016 x 0.022 inches rectangular wire from the Ultimate Wireforms Company. In this case, the displacement was observed to be 3.2 mm as the striker was placed 0.1 mm above the wire.

Table 19: Type of NiTi wire and load (g) in unloading process for 0.012 inch round wires at ISO setting

		Unloading force (g) at different locations(mm)							
		3		2		1		0.5	
Wire Brand	Type	Mean	Std	Mean	Std	Mean	Std	Mean	Std
Ortho organisers	SE	102.84085	1.84840	100.13085	0.40432	98.84333	0.41111	61.33450	0.53478
Ultimate Wires	SE	79.33852	2.38394	74.60460	1.02330	72.11257	0.82370	37.85595	0.33450

SE- super elastic

Table 20: Type of NiTi wire and load (g) in unloading process for 0.016 x 0.022 inch rectangular wires at ISO setting

		Unloading force (g) at different locations(mm)							
		3		2		1		0.5	
Wire Brand	Type	Mean	Std	Mean	Std	Mean	Std	Mean	Std
Ortho organisers	SE	438.21591	3.46708	385.99064	3.98465	351.07528	4.64601	295.69201	3.94857
Ultimate Wires	SE	392.86324	3.56720	340.87965	3.56794	324.58122	3.99047	317.51138	2.34650

As illustrated in Table 19, the unloading loads were compared for 0.012 inches of two different companies, namely, Ortho Organizers and Ultimate Wireforms for recommended ISO setting. The results of 1 factor ANOVA showed P value 0.119 > 0.05, there was no significant difference in the mean values of unloading loads 0.012 inch round wire. As seen from Table 20, 0.016 x 0.022 inch rectangular wires did not show any significant difference in unloading mean values for both the company wires with P value 0.512 which is greater than 0.05.

3.4.3 ANSI testing

Figure 27 and 28 show the load/displacement results of ANSI setting for 3 brands of rectangular wires and 3 brands of round wires from Ortho Organizers. It was observed that with changing size of the wires, the load/deflection curve changed drastically. The striker was placed 0.1 mm above the wire to hold the rectangular wire firmly.

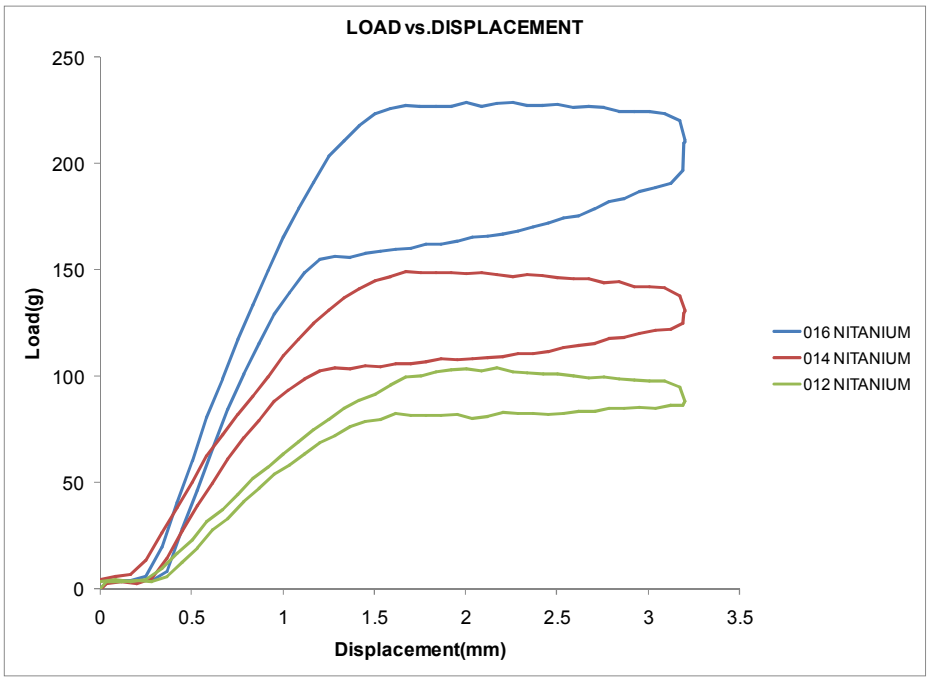

Figure 27: ANSI testing comparison of load/displacement curves of 3 rectangular wires

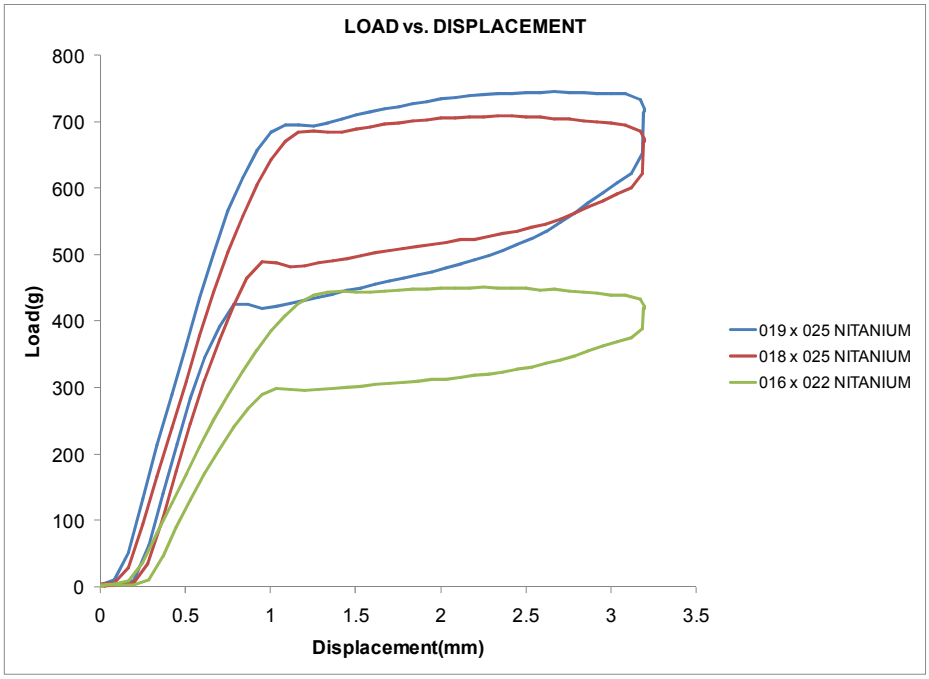

Figure 28: ANSI testing comparison of load/displacement curves of 3 round wires

Table 21: Unloading bending forces at 4 different locations for 6 different sizes of Ortho Organizers in ANSI setting

Wire size(in)	Unloading forces (g) at different locations (mm)							
	3.0000		2.0000		1.0000		0.5000	
	Mean	Std	Mean	Std	Mean	Std	Mean	Std
019 x 025	608.0120	14.3575	485.9327	12.3468	426.5349	10.9384	345.8563	7.8365
018 x 025	591.3450	22.0347	518.3547	11.2354	483.8460	9.7460	311.2364	8.4750
016 x 022	375.3465	6.3460	315.3465	5.4756	293.4536	4.2304	171.3364	2.3640
16.0000	223.3030	4.0871	165.7243	3.8564	148.5524	2.3451	65.9234	1.3456
14.0000	121.8123	2.1023	108.5430	2.8564	98.5823	2.1250	49.6093	2.3485
12.0000	85.0890	2.3649	81.1235	1.0465	63.4988	1.4111	27.5834	0.6458

The bending force during the unloading process was determined from load/displacement curves and reported in Table 21, where the 0.019 x 0.025 was found to have a maximum force of 608.0120g at 3mm with a standard deviation of 14.3575g and the 0.012 inch wire had the minimum force of 85.0890g at 3mm. Figure 29 shows the load/displacement curves of 0.012 inch round wire and 0.016 x 0.022 inch rectangular wire of Ultimate Wireforms Company.

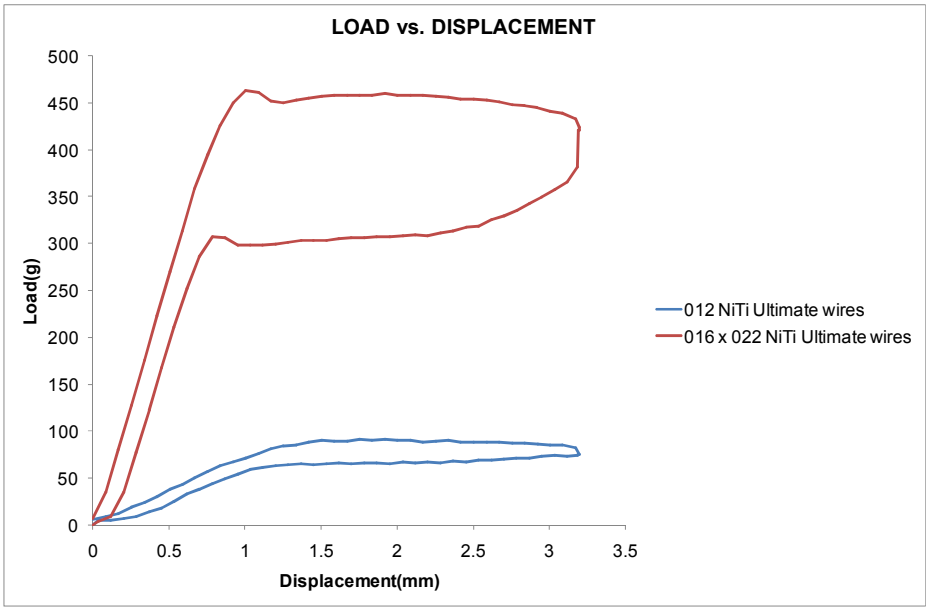

Figure 29: Comparison of load/displacement curves of rectangular 016 x022 and 012 round ultimate wires in ANSI setting

Table 22: Type of NiTi wire and load (g) in unloading process for 0.012 inch round wires at ISO setting

		Unloading force (g) at different locations(mm)							
		3		2		1		0.5	
Wire Brand	Type	Mean	Std	Mean	Std	Mean	Std	Mean	Std
Ortho organisers	SE	85.08895	2.36485	81.12354	1.04650	63.49875	1.41111	27.58340	0.64583
Ultimate Wires	SE	73.55725	2.12346	65.70642	2.11432	60.97274	1.26584	32.51308	0.45783

Table 23: Type of NiTi wire and load (g) in unloading process for 0.016 x 0.022 inch rectangular wires at ISO setting

		Unloading force (g) at different locations(mm)							
		3		2		1		0.5	
Wire Brand	Type	Mean	Std	Mean	Std	Mean	Std	Mean	Std
Ortho organisers	SE	375.34650	6.34600	315.34650	5.47563	293.45364	4.23040	171.33640	2.36400
Ultimate Wires	SE	357.48234	7.84637	308.71060	4.23320	298.46730	3.23650	251.92970	2.27384

In Table 22, the unloading loads from the ANSI testing were compared between 0.012 inch of two different companies: Ortho Organisers and Ultimate Wireforms. The results of one factor ANOVA gave a *P* value of 0.7384, which is greater than 0.05; therefore, there was no significant difference in their mean values. Mean bending forces for the 0.016 x 0.022 rectangular wire showed no significant difference in the unloading mean values of both the company wires with a *P* value 0.642 (> 0.05) as shown in Table 23.

3.3 Final Jacobian matrix validation

3.3.1 Set up 1 - Translation

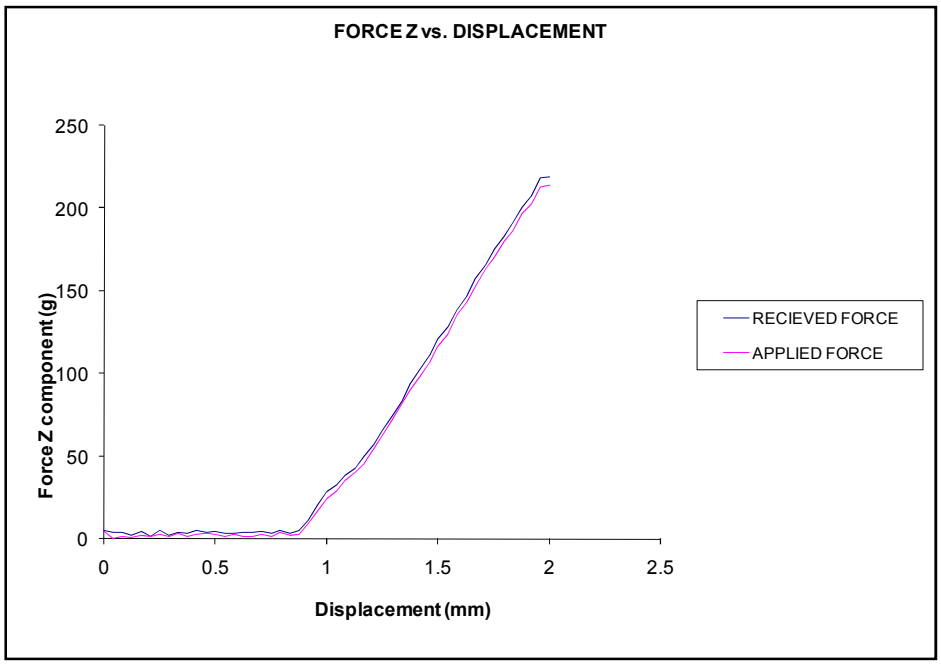

Figure 30: Comparison of Applied force vs. Received force along Z-direction

Figure 30 shows that the applied Z-component force, measured using sensor 7561 was equal to the received Z-component force measured using sensor 7560. Figures 31 and 32 demonstrates that the applied force in the X- and Y- components shows a similar pattern as that of the received force in the X- and Y-components.

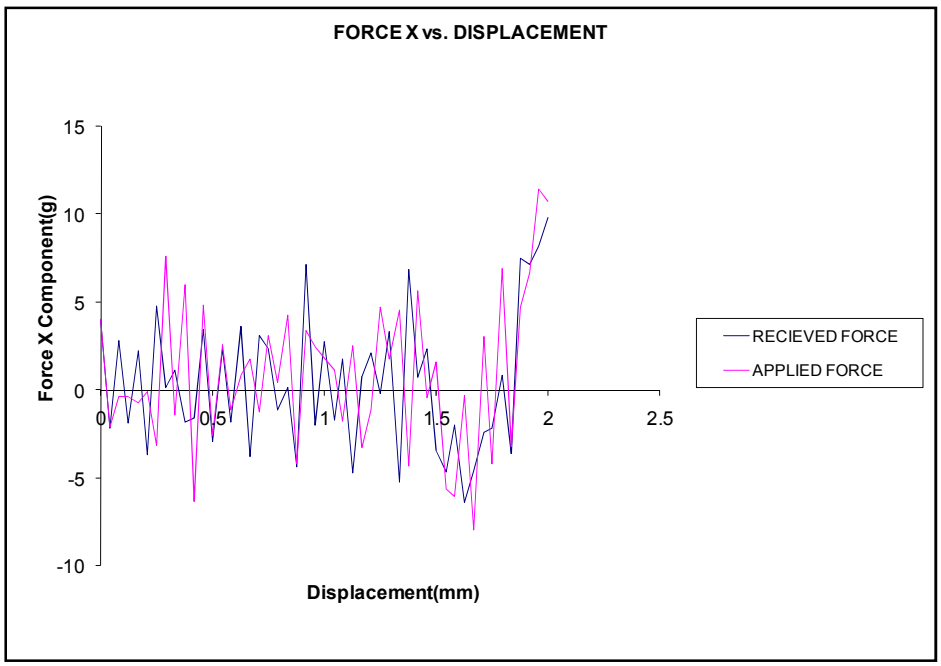

Figure 31: Comparison of applied force vs. received force along X-direction

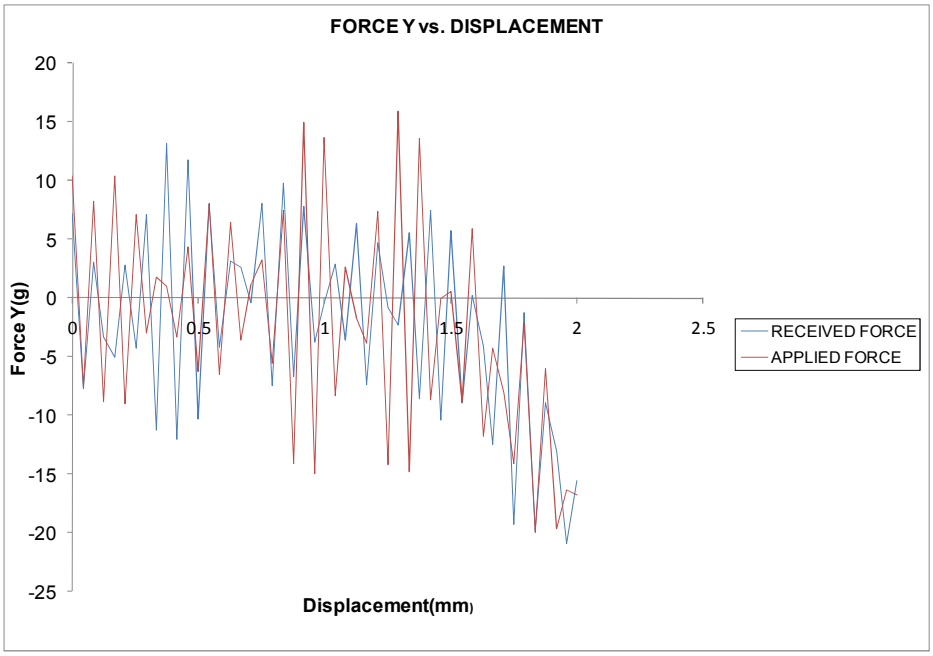

Figure 32: Comparison of applied force vs. received force along Y-direction

Figure 33 shows the torque values at point B (see Figure 21). It was observed that the expected torque values were aligned with actual torque values calculated after

multiplying with Jacobian matrix and demonstrates the validity of Jacobian matrix due to translation.

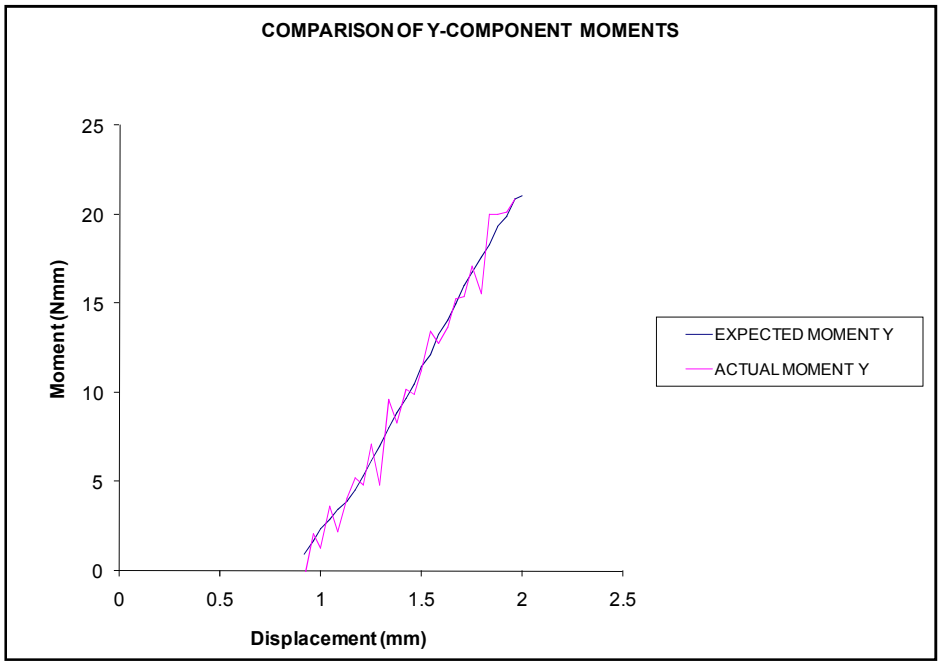

Figure 33: Expected torque Y vs. Actual torque at point B

3.3.2 Set up 2 - Rotational and Translation

Figures 34, 35, and 36 demonstrat that the applied force components show similar patterns to that of the received force components.

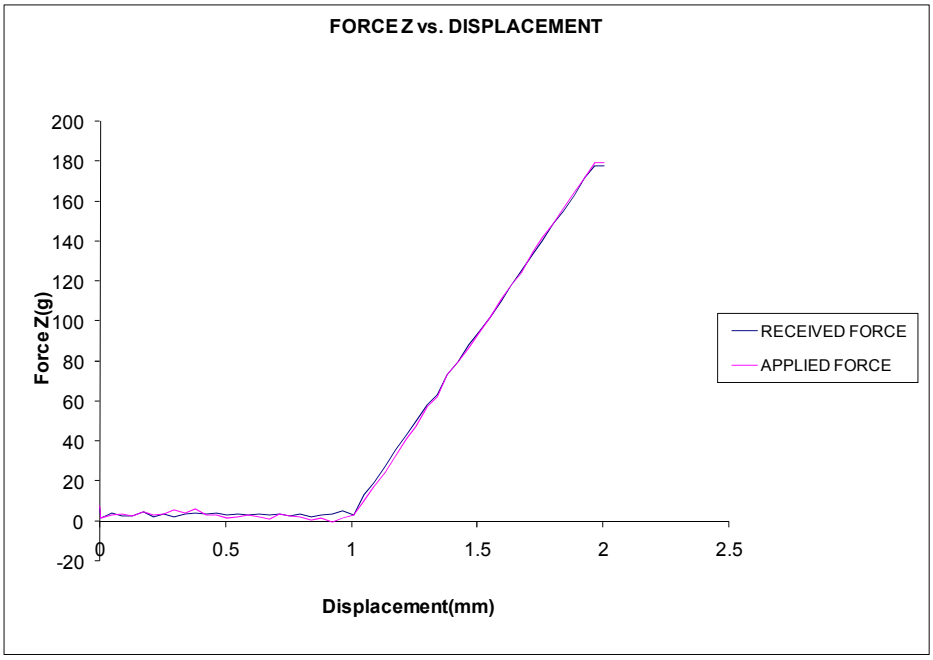

Figure 34: Comparison of applied vs. received force along Z-axis

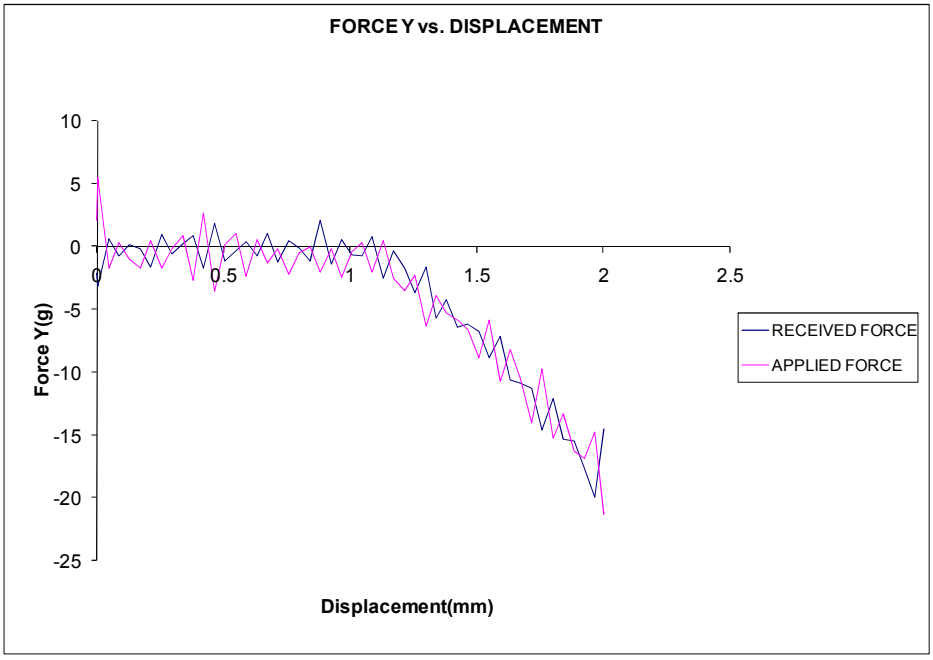

Figure 35: Comparison of applied force vs. received force in Y-direction

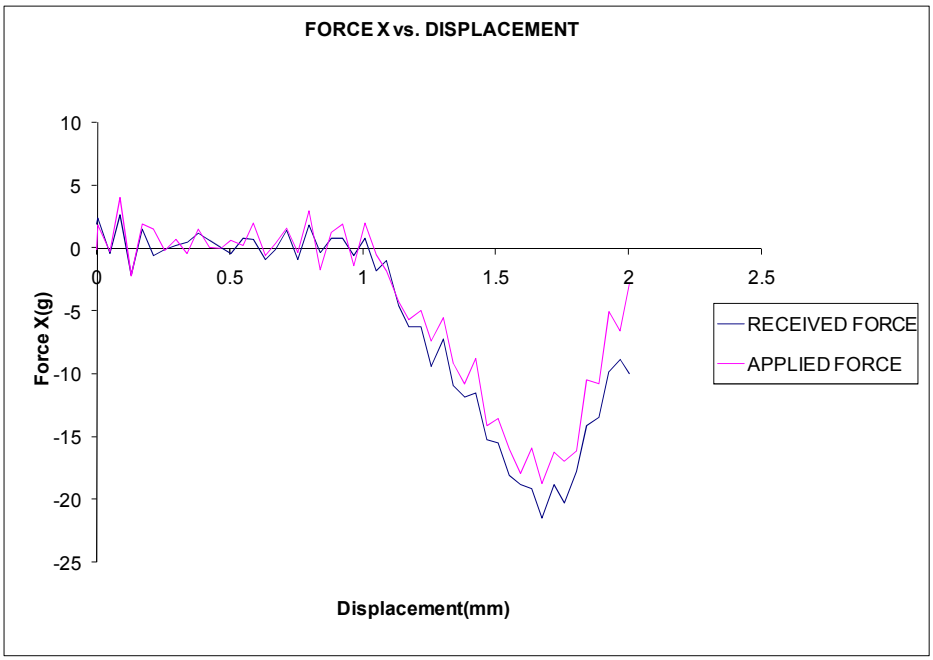

Figure 36: Comparison of applied force vs. received force along X-direction

Figure 37: Expected torque Y vs. actual torque Y at point B

As established in Figure 37, the expected torque about the Y-axis at point B shows similar pattern as that of actual torque values, which are obtained after applying the Jacobian matrix transformation.

4 Discussion

4.1 Sensor performance

Analyzing the accuracy level of the six degrees of freedom of the force/torque sensors was the principle criterion for developing orthodontic wire tester. The results obtained from the preliminary and final sensor verifications demonstrated its capabilities. The performance of the sensors was enhanced gradually by considering various parameters, which are discussed in following sections.

4.1.1 Preliminary individual axis load testing

The values obtained in the preliminary tests helped to understand the characteristics of these complex sensors. Table 9 demonstrates the variability in the measurement of force values where, for an expected 100g value on Y axis, the value obtained was 110.54 g with standard deviation of 19.9g. Apart from a 100g of a known weight, 2, 5, 10, 50, 200, and 500g were used for the same testing procedure and it was noticed that there was high variability in the measurement of the force values. There was a 10% error from the expected force value in both of the sensors. The reason for the variability was analyzed extensively, in order to determine the cause. During the early stages of sensor measurement program, the unloaded and loaded voltage values were noted down manually. Each time a value was manually noted, the program was stopped and then restarted. Since the measurement was not continuous, the unloaded voltage values changed each time the program was restarted. Another possible source of variation was originating from the 12V power supply, which was connected to the sensors at a much higher voltage level than the manufacturer's recommendation of 5V. In order to

minimize the error in the measurement, various parameters, including the testing procedure, filter setting, sampling rate, and voltage regulation, were taken into consideration and investigated.

4.1.2 Filter vs. Force measurement

The noise was considered to be a major limitation in this device and it was managed through different strategies. Understanding the influence of the low pass filters in LabVIEW was important, since there were no hardware-based low pass filters or signal amplifiers used with ATI force sensors.

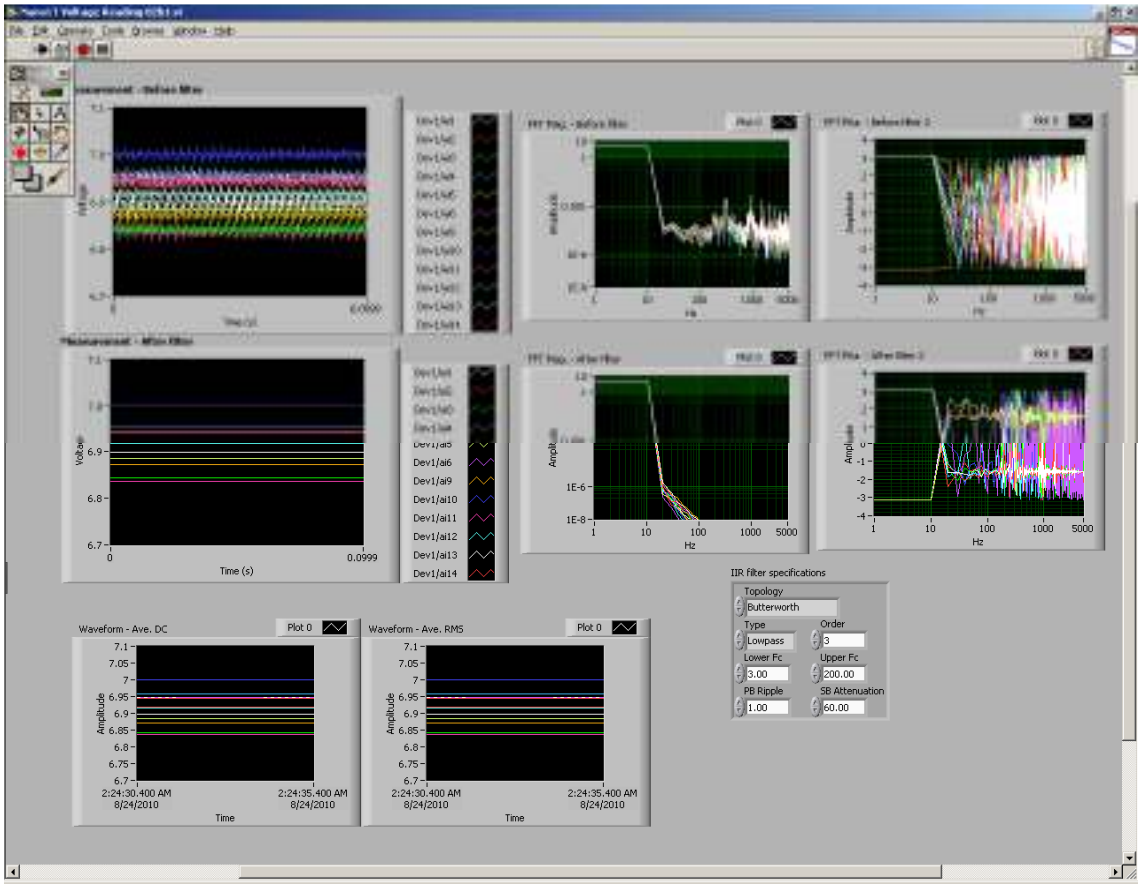

Figure 38: Front panel of the filter testing program

For choosing an optimum software filter configuration, numerous tests were performed using a filter testing program as shown in Figure 38. The unloaded voltage measurement values were analyzed before and after each filter setting. A Finite Impulse Response (FIR) filter is a type of signal processing technique whose impulse response stays for finite period of time. Initially, FIR filter was applied and the magnitude and phase response were analyzed using a Fast Fourier transform (FFT) program in LabVIEW as shown in Figure 38. It was noted for every case there was no appreciable change in the voltage values before and after the filter setting. The Infinite Impulse Response (IIR) filter has an internal feedback and an indefinitely present impulse response and was subsequently chosen to analyze the magnitude and phase responses. A 3rd oder Butterworth low pass IIR filter with a cutoff frequency of 3 Hz yielded the best results with minimal noise.

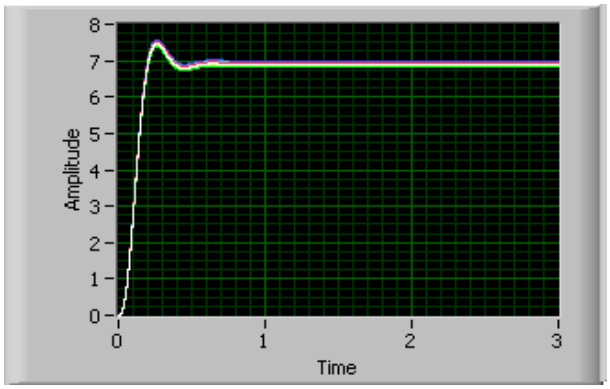

Figure 39: Initial unloaded measurement graph after passing through IIR filter setting for both the sensors (from front panel of Labview VI)

Even though the noise element was reduced significantly after the application of the IIR filter, an initial overshoot was observed at approximately 0.4 seconds, as shown in Figure 39. This overshoot was observed to cause the unloaded voltage values to shift

from its original value for a brief period of time. Since the force measurements were based on the difference of loaded and unloaded measurements, the overshoot influences the force reading significantly. After extensively analyzing the IIR filter, this phenomenon of overshoot was observed for all the measurements. It was observed that after the brief overshoot, the unloaded values settled down to a constant value with very little standard deviation. The problem of overshoot was addressed by eliminating the initial samples for unloaded measurement using the LabVIEW block diagram as shown in Figure 40.

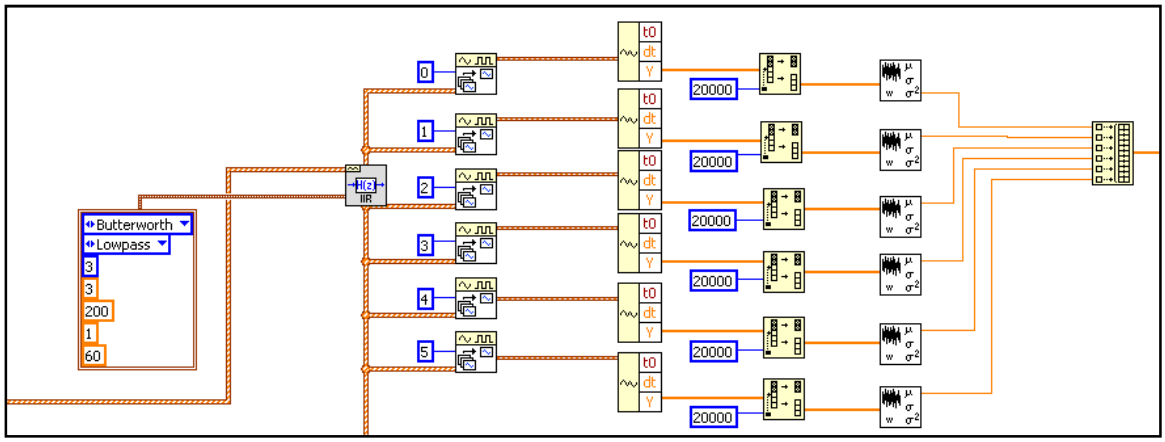

Figure 40: Block diagram of section of filter testing program for eliminating overshoot.

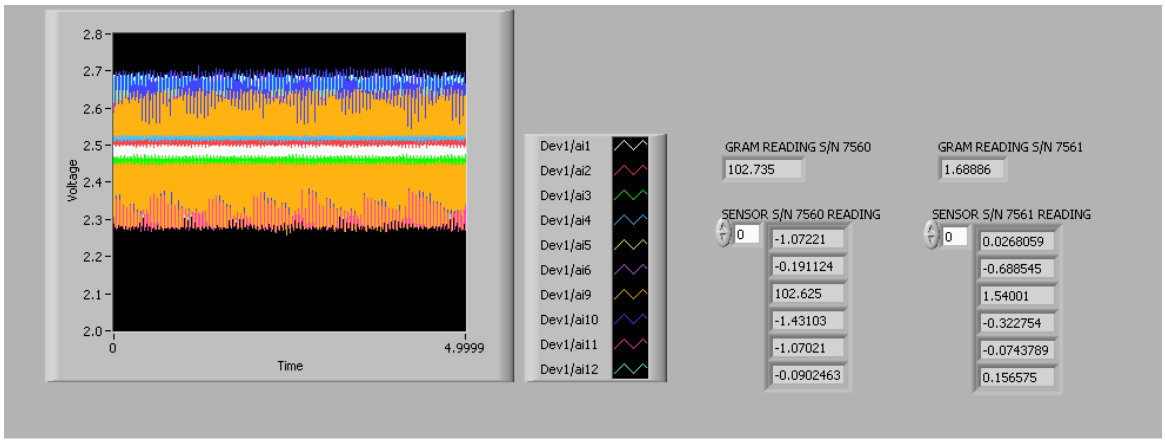

Figure 41: Front panel of the sensor measurement program without IIR filter setting

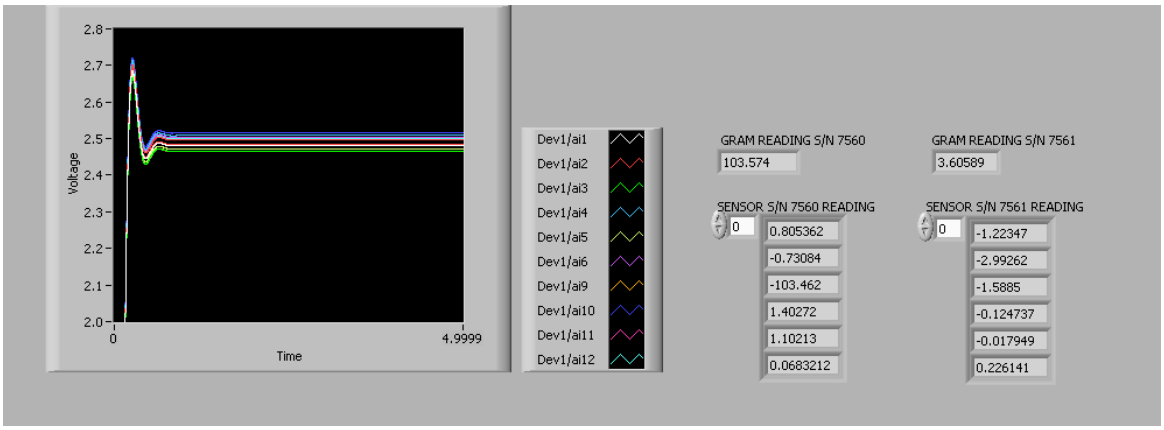

Figure 42: Front panel of sensor measurement program with IIR filter setting

Figures 41 and 42 shows the front panel of the sensor measurement program for examining forces with, and without, the IIR filter and no significant changes in the values were observed at a 95% confidence level. As force/torque measurements were obtained using the difference in loaded and unloaded values, the noise element associated without the IIR filter were cancelled out and does not influence the force/torque measurements.

4.1.3 Sampling rate vs. force measurement

Sampling rate is defined as the number of samples per unit time or (Hz) and the inverse of sampling rate is defined as number of samples obtained over the span of unit time. In earlier tests, the sampling rate was chosen at 10 kHz, which translates to a sample taken every 0.0006 seconds. Initially a higher sampling rate was used to investigate its influence on signal noise.

Experiments were performed to check the effect of sampling rate on the force measurements. The analysis were carried out using a LabVIEW program that was capable of continuous measurement of loaded and unloaded values. After incorporating the calibration matrix program with the basic sensor measurement program, the force/

torque measurements were captured continuously for 5 seconds which changed the testing procedure completely from the preliminary testing. Results from Table 4 show that there was no effect of sampling rate on force measurements as determined by a t-test with a 95% confidence level. At this point, the optimization of the sampling rate was not possible with the results obtained in Tables 10 and 11 and since, all the four sampling rates showed no difference in force measurement, the 10,000 Hz sampling rate was chosen for subsequent tests. Apart from sampling rate, the number of samples read also plays a part in the sensor measurement and the LabVIEW programming for sensor measurement was designed based on the conceptual working of sensors as explained in the Figure 8, where a while loop was essential for measuring the loaded voltage values. The force/torque values were measured for each loop in the program and for each loop, a certain number of samples had to be specified for reading the loaded measurement was optimized to 5000 samples per loop.

Ultimately, the filter setting, sampling rate, and number of samples to read were the parameters analyzed extensively and adjusted to reduce the noise component of the voltage fluctuation.

4.1.3 Final sensor program verification

The accuracy level of the sensor was tested using the optimized parameters, which were discussed in section 2.2.1.2. With load applied over the Z-axis only, the force along X and Y axis should be very close to zero. According to the manufacturers of the sensors the resolution range is 1/80 of a Newton, which is equivalent to 1.27g. This means that the minimum value that it can sense is 1.27g. From Tables 14 & 15, most of

the force values along X and Y axis were less than 1.27g, except when the higher weights were applied.

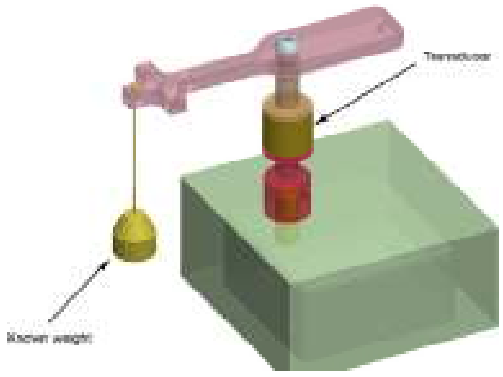

Figure 43: Calibration set up for sensors (Badawi et al., 2009)

Badawi et al., (2009) used the same ATI force sensor followed different method for calibrating. They applied load over the individual axis using a setup shown in Figure 43. They make no mention of the sampling rate, filter setting, and their sensor measurement program. The overall error calculated with our sensor and setup was 0.5%. According to Badawi (2009), the overall error observed when loaded over the Z-axis was 1.75%. Thus, the overall sensor performance was vastly improved using the sensor measurement program and proper test conditions of this device.

4.2 Motor Performance

Table 16 shows the error percentage of velocity was less than 0.05% proving that the accuracy of the stepper motor was extremely high. A ruler was used to verify the displacement by visual monitoring, so there could be a significant occurrence of human error associated with this verification. The important task of the application was to develop a device capable of plotting load and displacement curves. Generally, most of the motors working with closed loop mode require a feedback device for precise movement.

This stepper motor works well with open loop mode with no feedback and was observed to operate accurately, as shown by the results. Since the load capabilities of the stepper motor are far higher than the required application, it was assumed that it would move to the exact location through the specified number of pulses. By examining the pulse rate, number of pulses, and the revolutions per minute (RPM) values (from Table 16), it was observed that the motor behaves exactly according to the theoretical calculations.

The results discussed in previous sections demonstrate significant evidence for the accuracy of the sensors and motors.

4.3 Three point bending test

Nickel-titanium (NiTi) alloys have been widely used in orthodontics because of their favorable super elastic properties and their ability to provide a light continuous force for efficient tooth movement (Theodosia et al., 2007). Nickel-titanium wires of Ortho Organizers and Ultimate Wireforms were used to demonstrate the validity of the device. The unloading bending forces in Tables 18 and 21 have shown close resemblance with respect to the unloading bending force values provided by Ortho Organizers product specification brochure. Similarly, the unloading bending values from Ultimate Wireform's wires matched their specifications. Table 19 and 20 demonstrate the comparison between the wires of both the companies for two different wire sizes and proved that there was no significant difference between the mean unloaded bending values.

4.3.1 ISO vs. ANSI standards

Figures 44 and 45 show the comparison of the load/displacement curves for ANSI and ISO setting for the 0.016 x 0.022 and 0.012 sizes of Ultimate Wireform wires. As discussed in Section 1.3, the results provided here show the loading portion of the graphs, which simulates the activation of the wire, and the unloading segment of the graph, which provides information on forces associated with the wire as it undergoes deactivation. The unloading forces associated with the wire provide an indication of its potential clinical behavior. From Figures 44 and 45, it was observed that the loading curve from the ISO setting is higher than that of the ANSI setting.

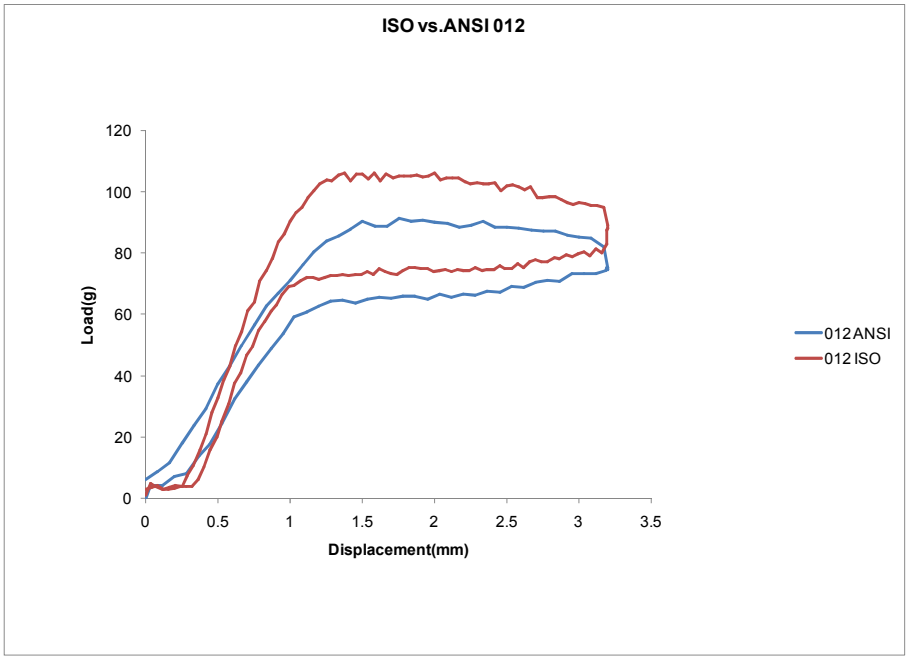

Figure 44: Comparison of load/displacement curves of ISO vs. ANSI of 016 x 022 ultimate wires

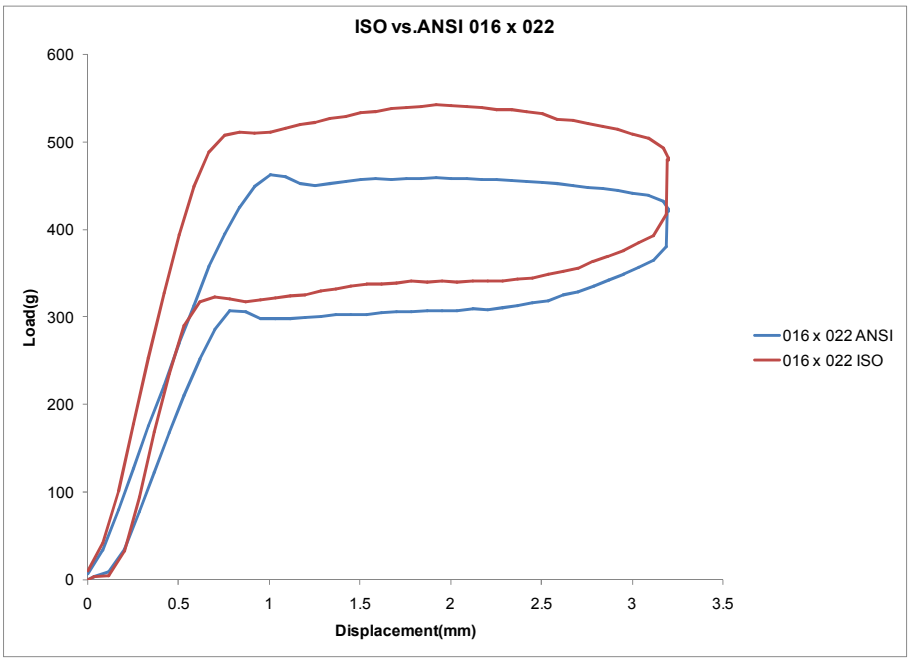

Figure 45: Comparison of load/displacement curves of ISO vs. ANSI of 012 ultimate wires

One factor ANOVA was performed between the loading curves and unloading curves for both the wires. Table 24 shows the P values of loading and unloading curves at 95% confidence level and a significant difference was observed in the loading curves of 0.016 x 0.022 (*P* value 0.016), while all other *P* value show no significant differences.

Table 24: Comparison of P value of loading and unloading curves of 016 x 022 and 012 wires

	Loading P Value	Unloading P Value
016 x 022	0.016	0.21
12	0.108	0.267

4.3.2 Effect of velocity

Other important parameters, such as the influence of velocity on the three point bending test, were also analyzed in this study. Figures 46 and 47 illustrate the comparison of the 0.016 inch and 0.016 x 0.022 wires, from Ortho Organizers, at three different speeds. It was observed that there were no significant differences with the three speed values on the three point bending test at *P* values higher than 0.05 for both the wires. It

was observed that by lowering motor speed, the measurements became finer, while an increased speed resulted in coarse measurements.

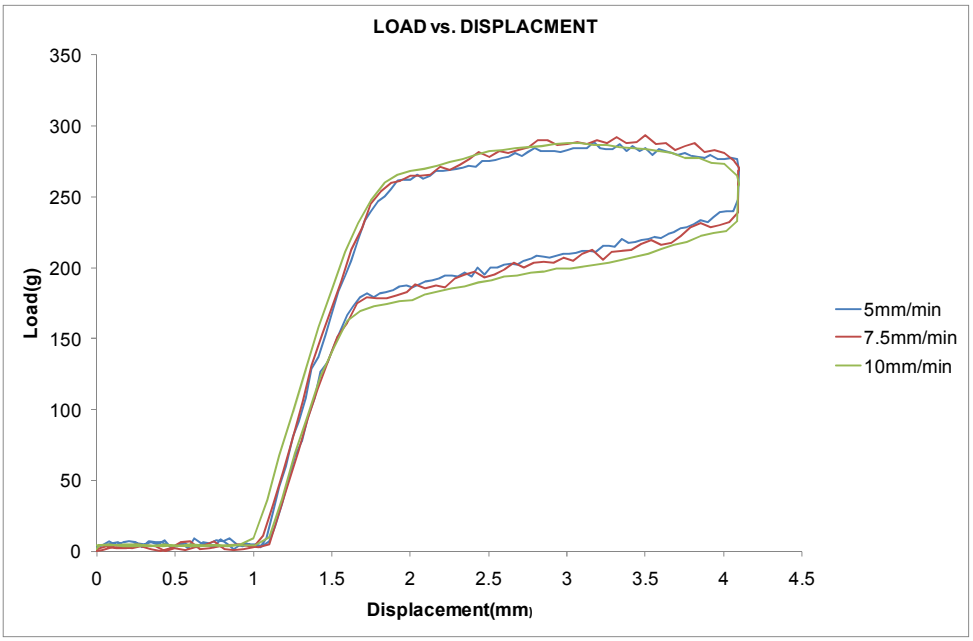

Figure 46: Comparison of load/displacement curve at ISO setting of 016 inches Ortho Organizer wire at three different speeds.

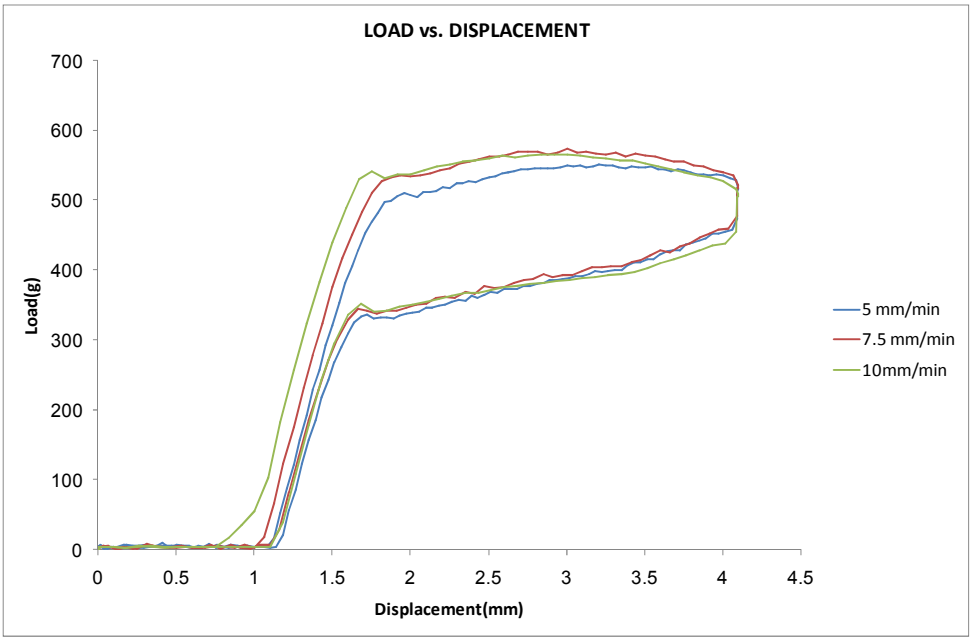

Figure 47: Comparison of load/displacement curve at ISO setting of 016 x 022 inches Ortho Organizer wire at three different speeds.

From the previous studies, a high degree of variability existed amongst the researchers for choosing an optimum velocity for three point bending test: Oltjen et al., (1995) studied the three point bending test at 1.27mm/min, Shima et al., (2002) did not mention any velocity, Kapila et al., (1992) followed 1mm/min, and Theodosia et al., (2007) performed the study at 0.1mm/min. In order to correlate the three point bending tests with clinical studies, previous researchers tried to use lower velocities that closely resemble the speed of the tooth movement. From the results of this studies it was determined that slower velocities do not influence the three point bending test measurements. Another important factor observed from the previous studies was that the researchers hardly followed ANSI and ISO standards for correlating three point bending test with clinical applications. The ANSI and ISO standards are mainly followed by wire manufacturers and that is the reason why it was hard to compare the results from this study with the results from previous researchers.

According to the New American Dental Association (ADA) Specification Number 32 orthodontic wires three point bending tests are the standard method for evaluating orthodontic wires. Many researchers questioned its direct clinical application. Segner et al., (1995) proposed that it was not possible to transfer the laboratory results of the three point bending test to the clinical orthodontic setting. They mentioned only patients with extreme irregularities experience deflections greater than 1mm. Brantley et al., (2001) described in routine orthodontic treatment that the deformation of NiTi wires was not sufficient to take advantage of their super elastic behavior. They also told that the three point bending had been employed as a physical property test. It was a method focusing more on the physical and biomechanical properties of the wire and was useful

mainly for theoretical evaluations. Segner et al., (1995) mentioned that in a clinical setting, it was almost impossible to assess the strain exerted on the wire. According to them, friction increases the effective force in the loading process and decreases in the unloading process causing the load/deflection curve to get distorted. With these shortcomings of three point bending test, factors such as friction should be considered for effective evaluation.

4.4 Jacobian Validations

Hisham et al., (2009) demonstrated the use of Jacobian transformations to transform force systems exactly at the location of teeth, but they never showed the validation of the matrix. To prove the validity of Jacobian matrix, different strategies and experimental set ups were designed. Initially, Jacobian matrixes were derived for the test conditions shown in Table 6 (refer section 2.4) using the equations discussed in Section 1.4. The validity of Equation (20) was tested with a preliminary Jacobian setting and it was observed that the equation did not hold and the values did not match due to the errors in the sign conventions of the sensors. With the results from the preliminary setting, it was concluded that the experimental set up was not proper. In the preliminary set up, the point of application of force was directly over sensor 7561. The torque components measured by the sensor were nearly zero and it made it impossible to transform values from sensor 7560. A new experimental set up was designed to resemble the teeth set up (refer section 2.4.1) and used the motor to applying a force for validating the Jacobian matrix. Figures 30, 31, and 32 demonstrate the set up used to test the Jacobian matrix for only translation of a perfectly rigid body. It was clearly seen that the applied force, which

was measured using sensor 7561, was equal to the received force measured by sensor 7560, which was a major assumption for the derivation of Jacobian matrix. Since it was proved that for a perfectly rigid body, according to the free body diagram, the forces acting at points A, B and C in Figure 20 are equal due to the total summation of forces in all the three directions being zero.

$$f_{x1} = f_{bx} = f_x \tag{34}$$

$$f_{y1} = f_{by} = f_y \tag{35}$$

$$f_{z1} = f_{bz} = f_z \tag{36}$$

The values which change with translation are the torque values. Since the major applied force is at Z direction only, the torque values around the Y axis would change linearly with distance. As illustrated in Figure 32, the expected torque values at point B were aligned with the actual torque values that were calculated after multiplying with the Jacobian matrix. This proves that the Jacobian matrix derived with the translation vector is valid.

Figure 34, 35, and 36 proved that Equations (34), (35) and (36) hold true. That is, the applied force values were equal to the received force values in all the three directions and thereby proving that the setup was rigid. The forces could be compared irrespective of the rotation of the sensor along Z direction; In Figure 36, the expected torque along Y-axis at point B (Figure 21) showed the similar pattern as that of actual torque values, which were calculated after multiplying with Jacobian matrix. This proved the validity of Jacobian matrix due to both translation and rotation.

5. Conclusion

Despite the earlier development of a few orthodontic three-dimensional wire simulators, none of them were developed to perform a variety of applications. The device developed in this thesis has flexible capabilities to help understand and analyze several orthodontic clinical issues at an effective cost. The three point bending test, which is one of the most important applications of this device, was developed and is detailed in this thesis. The orthodontic wire tester was also configured to be able to perform a three point bending test in accordance with the International (ISO) and American (ANSI) standards.

The degree of testing error determined during device validation, which was performed using Ni-Ti wires from two different manufacturers, closely correlated with the specified unloaded bending force values provided by the manufacturers. The error associated with the force/torque sensor measurements was minimized and the error associated with the velocity of stepper motor was found to be 0.05% or less, which demonstrates a high level of device accuracy. In addition, a new setup was developed in order to validate and establish the Jacobian transformations that allow for the measurement of the forces and torques at desired locations (e.g., tooth locations) in this device. Finally, comparative studies of the two standardized three point bending tests (i.e., ISO and ANSI) were performed and the results showed that there were no significant differences in the load/displacement curves, which further demonstrated device efficacy.

This device will allow the user to perform modified three point bending tests by incorporating different sets of brackets, archwires, and/or ligations. In addition, many types of orthodontic clinical scenarios, including fully, or partially fixed, appliances, can

be readily simulated and studied. Data from this device can also assist in building accurate and realistic computer models for the simulation and prediction of orthodontic tooth movement. In summary, the development of a system for understanding the biomechanical factors of orthodontic treatment opens up new avenues for the investigation of specific clinical issues, which will prove to be avaluable resource in future treatment processes.

References

1. ISO 15841:2006(E), (2006) “Dentistry- wire for use in orthodontics” First edition, Geneva, Switzerland.

2. ANSI/ADA Specification No. 32, (2000). “Orthodontic Wires”. American Dental Association, Chicago, IL.

3. Nanda R, Kuhlberg A. (2005) "Principles of Biomechanics." Biomechanics and Esthetic Strategies in Clinical Orthodontics”. Elsevier All Rights Reserved . 1-16. Print.

4. Garrec, P., & Jordan, L. (2004). “Stiffness in bending of a superelastic ni-ti orthodontic wire as a function of cross-sectional dimension”. Angle Orthodontist, 74(5), 691-696.

5. Huang, Z. -., Gopal, R., Fujihara, K., Ramakrishna, S., Loh, P. L., Foong, W. C., Ganesh, V. K., & Chew, C. L. (2003). “Fabrication of a new composite orthodontic archwire and validation by a bridging micromechanics model”. Biomaterials, 24(17), 2941-2953.

6. Oltjen, J. M., Duncanson Jr., M. G., Ghosh, J., Nanda, R. S., & Currier, G. F. (1997). “Stiffness-deflection behavior of selected orthodontic wires”. Angle Orthodontist, 67(3), 209-218.

7. Iijima, M., Ohno, H., Kawashima, I., Endo, K., & Mizoguchi, I. (2002). “Mechanical behavior at different temperatures and stresses for superelastic nickel-titanium orthodontic wires having different transformation temperatures”. Dental Materials, 18(1), 88-93.

8. Koenig, H. A., & Burstone, C. J. (1974). “Analysis of generalized curved beams for orthodontic applications”. Journal of Biomechanics, 7(5), 429-435.

9. Bednar, J. R., Gruendeman, G. W., & Sandrik, J. L. (1991). “A comparative study of frictional forces between orthodontic brackets and arch wires”. American Journal of Orthodontics and Dentofacial Orthopedics : 100(6), 513-522.

10. Walker, M. P., Ries, D., Kula, M., & Fricke, B. (2007). “Mechanical properties and surface characterization of beta titanium and stainless steel orthodontic wire following topical fluoride treatment”. Angle Orthodontist, 77(2), 342-348.

11. Kasuya, S., Nagasaka, S., Hanyuda, A., Ishimura, S., & Hirashita, A. (2007). “The effect of ligation on the load-deflection characteristics of nickel-titanium orthodontic wire”. European Journal of Orthodontics, 29(6), 578-582.

12. Kapila S, Reichhold, Anderson R S, and Watanabe L (1991). "Effects of Clinical Recycling on Mechanical Properties of Nickel-titanium Alloy Wires". Am J Orthod Dentofac Orthop, San Francisco, Concord, and Castro Valley, California .

13. Krishnan V, Kumar K (2004). "Mechanical properties and surface characteristics of three archwire alloys". Angle Orthodontist, 74 825-831.

14. Kapila, S., Haugen, J. W., & Watanabe, L. G. (1992). "Load-deflection characteristics of nickel-titanium alloy wires after clinical recycling and dry heat sterilization". American Journal of Orthodontics and Dentofacial Orthopedics, 102(2), 120-126

15. Wilkinson P D, Dysart P S, Hood J A, Herbison G P (2002). "Load-deflection characteristics of superelastic nickel-titanium orthodontic wires".American Journal of Orthodontics and Dentofacial Orthopedics 121 483-495.

16. Nakano H, Satoh K, Norris R, Jin T, Kamegai T, Ishikawa F, Katsura H. (1999) " Mechanical properties of several nickel-titanium alloy wires in three-point bending tests". Am J Orthod Dentofacial orthop 115, 390-395.

17. Theodosia N, Senn C, Wichelhaus. (2007). "Load-Deflection Characteristics of Superelastic Nickel-Titanium Wires". Angle Orthodontist, Vol 77, No 6.

18. Bartzela, T. N., Senn, C., & Wichelhaus, A. (2007). "Load-deflection characteristics of superelastic nickel-titanium wires". Angle Orthodontist, 77(6), 991-998.

19. Shima, Y., Otsubo, K., Yoneyama, T., & Soma, K. (2002). "Anisotropic orthodontic force from the hollow super-elastic ti-ni alloy wire by transforming the wire cross-section". Journal of Materials Science: Materials in Medicine, 13(2), 197-202

20. Kusy, R. P., & Dilley, G. J. (1984). "Elastic modulus of a triple-stranded stainless steel arch wire via three- and four-point bending". Journal of Dental Research, 63(1), 1232-1240.

21. Badawi H, Toogood R,Carey J, Heo G, Major P.W (2009). "Three-dimensional orthodontic force measurements" Am J Orthod Dentofacial Orthop ;136:518-28

22. Hiromishi F, Livesay G, Fujita M, Woo F (1999). "Forces and moments in six-DOF at the human knee joint: Mathematical description for control" Journal of Biomechanics. Vol 29(12) 1577-1585.

23. Solonche, D. J., Burstone, C. J., & Vanderby Jr., R. (1977). "A device for determining the mechanical behavior of orthodontic appliances". IEEE Transactions on Biomedical Engineering, 24(6), 538-539.

24. Bourauel, C., Drescher, D., & Thier, M. (1992). “An experimental apparatus for the simulation of three-dimensional movements in orthodontics”. Journal of Biomedical Engineering, 14(5), 371-378.

25. Menghi C, Planert J, Melsen B.(1999) “3-D experimental identification of force systems from orthodontic loops activated for first order corrections”. Angle Orthod .

26. Miura, F., Mogi, M., Ohura, Y., & Hamanaka, H. (1986). “The super-elastic property of the japanese NiTi alloy wire for use in orthodontics”. American Journal of Orthodontics and Dentofacial Orthopedics, 90(1), 1-10.

27. Miyakawa, O., Shiokawa, N., Matsuura, T., & Hanada, K. (1985). “A new method for finite element simulation of orthodontic appliance-teeth-periodontium-alveolus system”. Journal of Biomechanics, 18(4), 277-284.

28. Oriental Motor Corp. (2010). “Motorized Actuators: Compact Linear Acuators”, Tokyo, Japan.

29. TDK Corp. (2010). “ Humidity Sensor Units: CHS Series”, Tokyo, Japan.

APPENDIX A: Three point bending test manual

1 INTRODUCTION

- This document provides instructions to get started with 3pt bending test program
- The program has wide capabilities for measurement of Load/Displacement curves
- The device is designed taking into account all required safety conditions
- Aim of the program is to simultaneously control the following motor and sensors:
    a) 2 force/torque sensors
    b) Stepper motor
    c) Humidity sensor
    d) Temperature sensor

2 CAUTION

- Operate the device only as specified in the manual. Improper usage can result in hazardous situations and extensive damage to the motor and sensors
- Do not substitute parts or modify the program.

3 GETTING STARTED WITH THREE POINT BENDING TEST PROGRAM

3.1 TEMPERATURE CONTROL

- **SWITCH ON** the unit before opening the program.
- Set the temperature of the unit if required (maximum of **50 degree Celsius).**
- **Switch on the fan (right button) and heater (left button)** as shown in the following.

Figure 20: Front panel of temperature control unit
21

- Speed of the fan could be set high or low by pressing the switch above or below respectively.

3.2 TESTING SETUP

- Can perform 3 point bending test according to standards ISO & ANSI

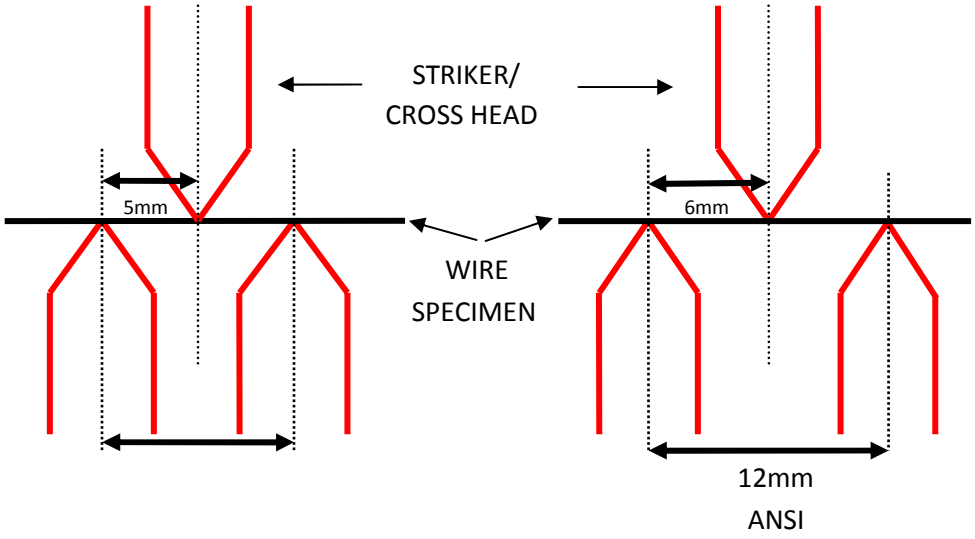

Figure 22: Different setting between ISO & ANSI

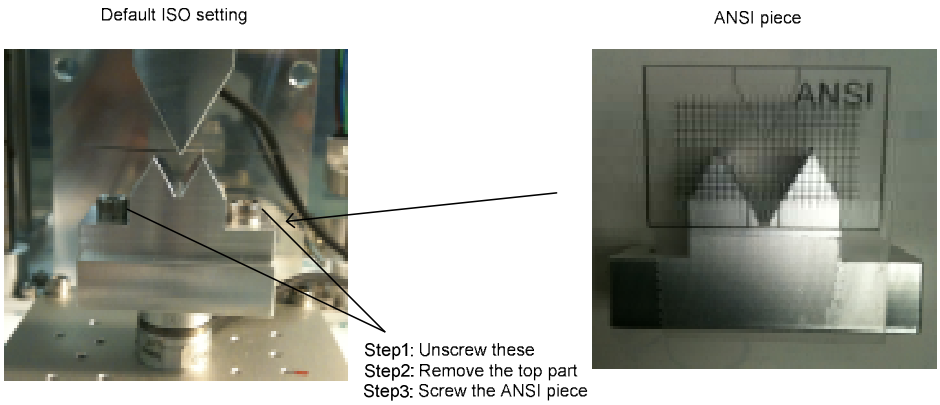

Figure 23: Changing the setup from ISO to ANSI

- The default setting will be kept for performing ISO testing as shown in Figure 3.
- Figure 3 demonstrates, changing the setting from ISO to ANSI standards.
- To ensure the wire reaches the required temperature, place the specimen wires inside the unit before testing.

- Place the wire to be tested in the testing set as shown in Figure 4.

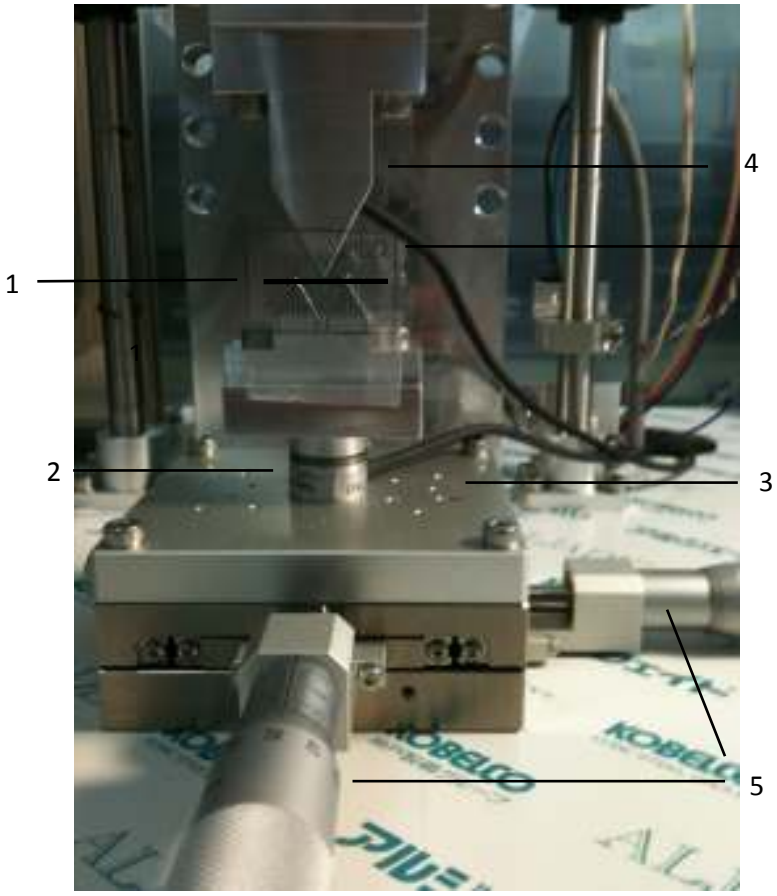

Figure 24: Wire placement location

1. Specimen wire
2. Sensor S/N 7560
3. XY stage
4. Striker
5. Calipers
6. ISO positioning sticker

- XY Stage aids in the movement in the X and Y direction and is controlled manually by rotating the calipers.

- Striker moves up and down in Z direction and is controlled by motor movement.

- ISO positioning stickers helps to locate the exact location, which is 1 mm above the wire to position the striker.

- Once the wire is ready and placed in the setup, close the doors and wait till the unit reaches the set temperature.

NOTE:

- Motor direction sense is explained in the following figure

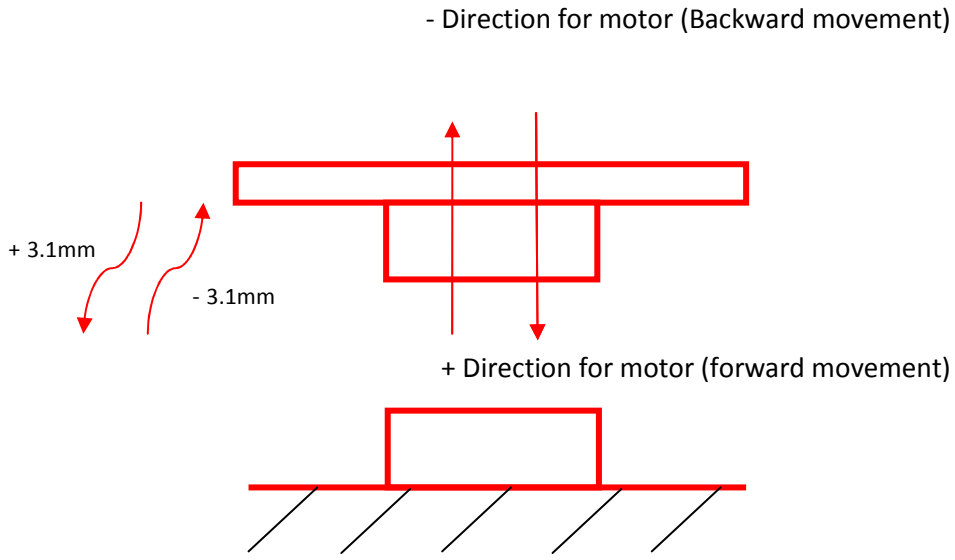

Figure 25: Motor movement direction

✓ Double click the icon named **"3 POINT BENDING TEST.VI"** in the desktop to open the program.

✓ LabVIEW window will show up and after few seconds the program will open and front panel shown in Figure 6 will appear.

PROGRAM CONTROLS

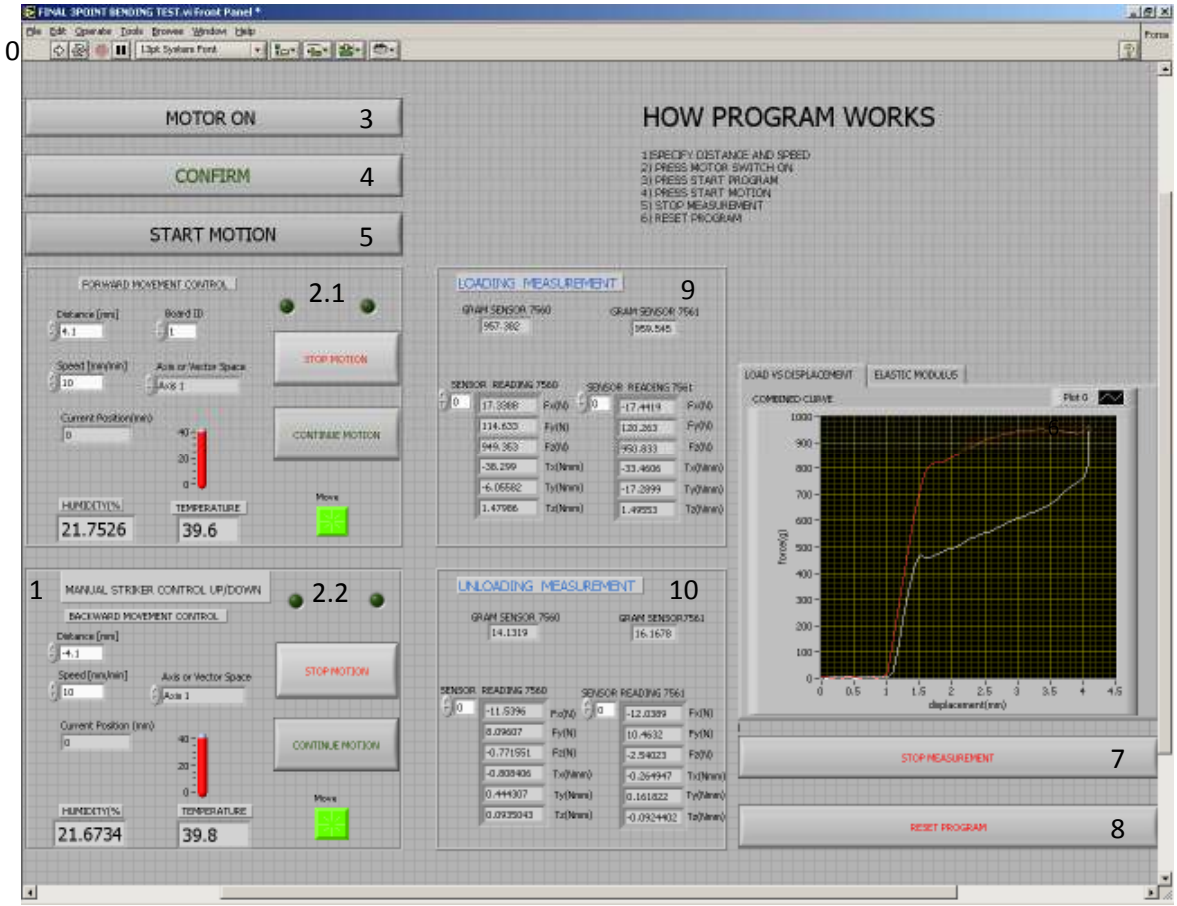

Figure 26: Front panel of 3 point bending test program

4 THREE POINT BENDING TEST PROGRAM FLOWCHART

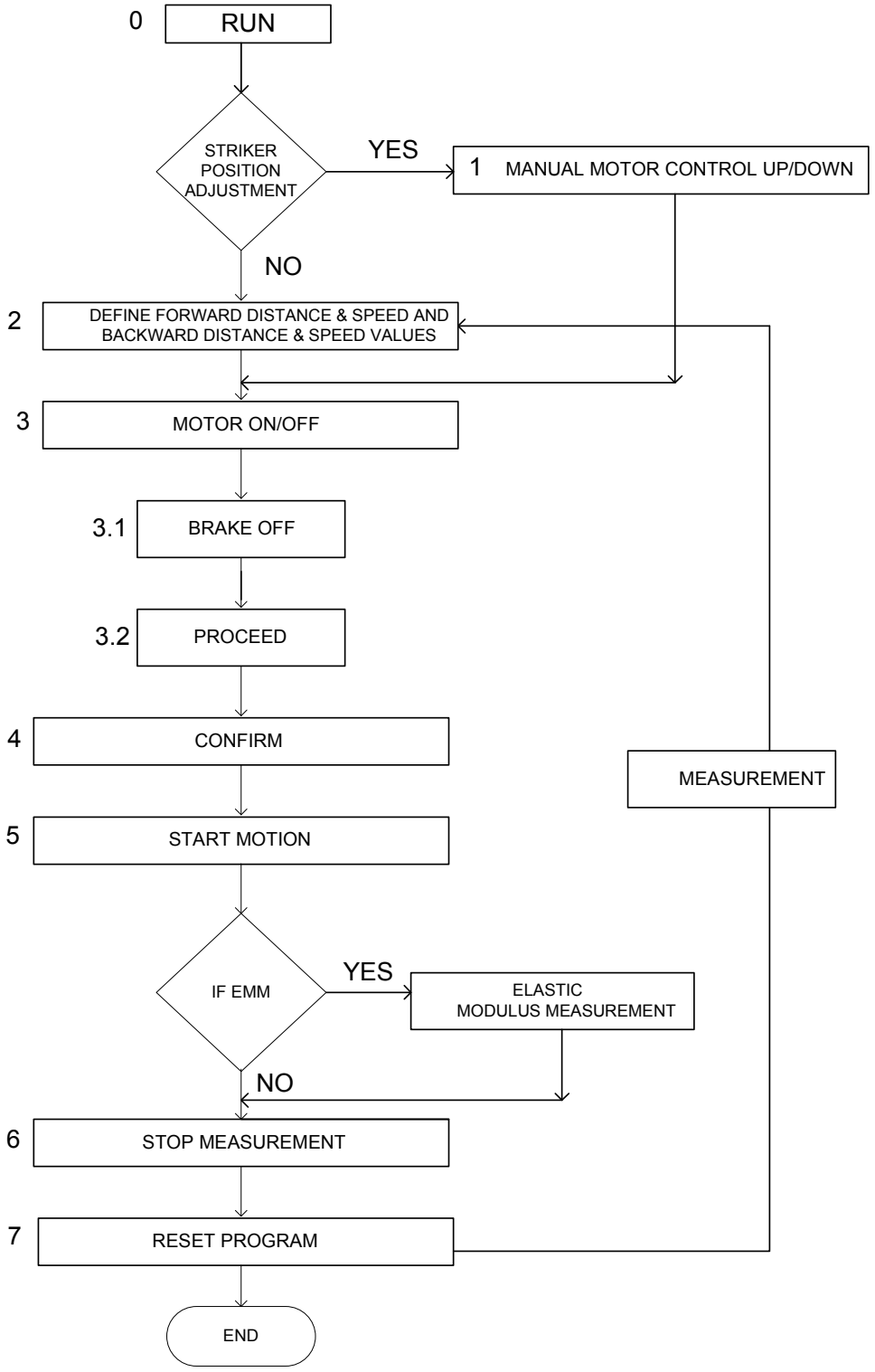

NOTE: These numbers mentioned here correspond to the program controls

5 DETAILED PROGRAM CONTROLS EXPLANATION

STEP 0: RUN THE PROGRAM

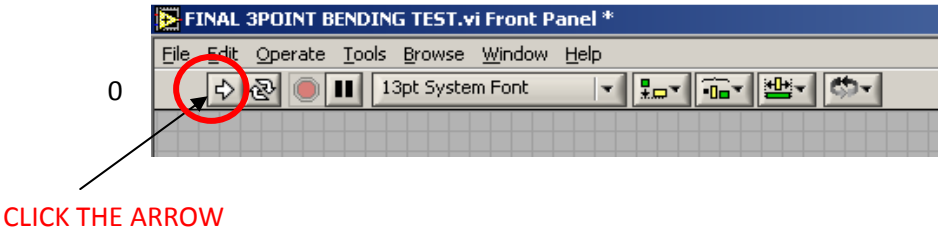

- ✓ To get started with test, click the above shown box

OPTIONAL (IF THE STRIKER IS POSITIONED PROPERLY SKIP THIS STEP AND GO TO STEP 2)

STEP 1: MANUAL MOTOR CONTROL

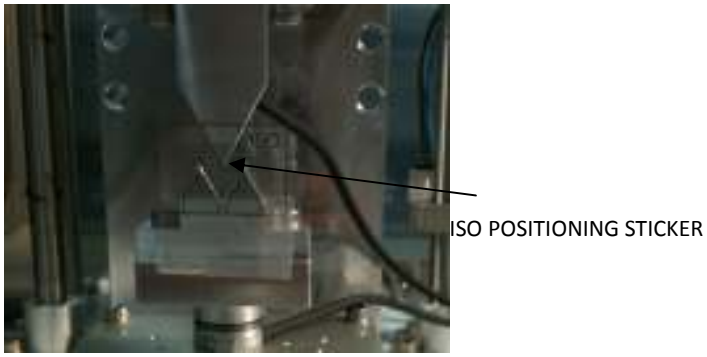

Figure 27: Positioning the striker indicated by the arrow

- ✓ If the striker is not positioned properly, accordingly adjust the striker up or down to place it exactly 1mm above the wire using the ISO positioning sticker, prior to starting the measurement.

- ✓ When performing the ANSI testing for rectangular wires, it is advisable to position the striker as close as possible to the specimen wire.

- ✓ It is important to define the distance and speed values to check if the motor is functioning properly as shown in block 1.

✓ Skip STEP 2 and go to STEP 3 and continue (See flowchart).

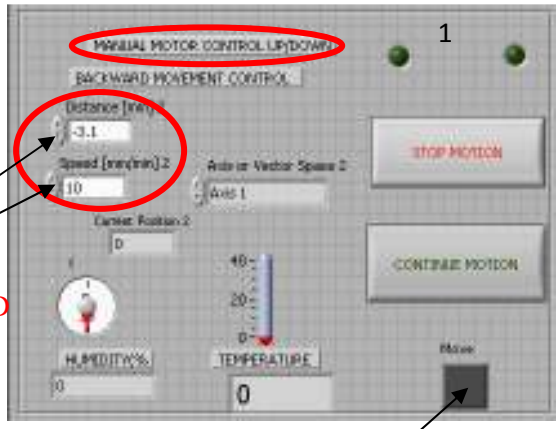

DEFINE THE DISTANCE AND SPEED

INDICATES MOVEMENT IS COMPLETE

Note: Specifying the speed value as zero will result in infinite speed to the specified distance and may result in damage to the motor

STEP 2: BEGIN MEASUREMENT

- ✓ According to the ISO and ANSI standards, there should be continuous measurement from the point where striker touches the specimen wire(0 mm location) to 3.1 mm forward and backward distances.
- ✓ It is not possible to position the striker exactly over the specimen(0 mm location)
- ✓ Even though there is positioning sticker it is important to determine the position where the striker is above the specimen wire.
- ✓ Perform the calibration step to determine the position.
- ✓ Specify the distance and speed of the striker movement

Example: To perform this operation

	Forward	Backward
Distance(mm)	4.1	4.1
Speed(mm/min)	10	10

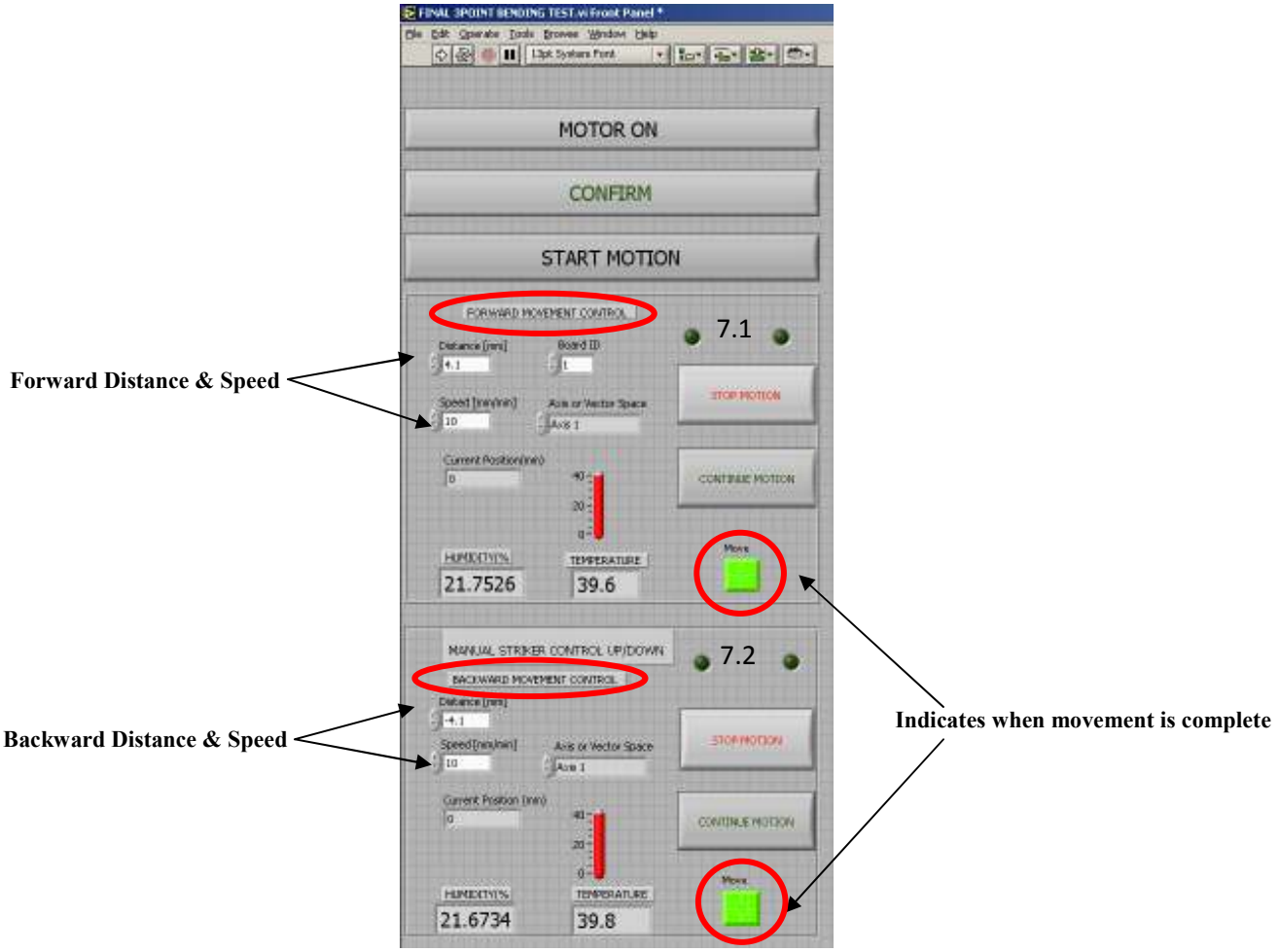

NOTE:

- Specifying the speed value as zero will result in infinite speed to the specified distance and may result in damage to motor.
- Resolution of the motor is set : 0.004mm
- Minimum advisable speed of the motor :0.4mm/min

- Different forward and backward distance & speed can be set up, example, to move 3mm forward at 10mm/min, and 5mm backward at 5mm/min.

- To stop the striker movement at any point of time, use the safety button STOP MOTION in both forward & backward movement control.

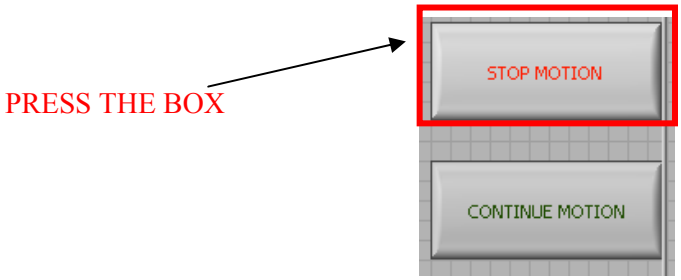

- To continue the movement, press the CONTINUE MOTION button.

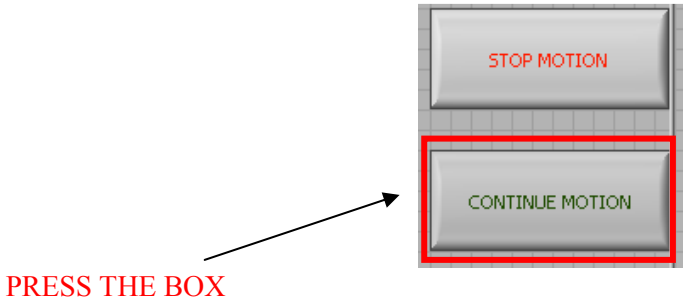

- The following sign indicates the current position of the Striker in millimeters.

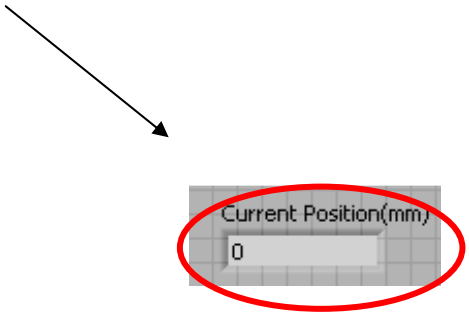

STEP 3: PRESS MOTOR SWITCH ON

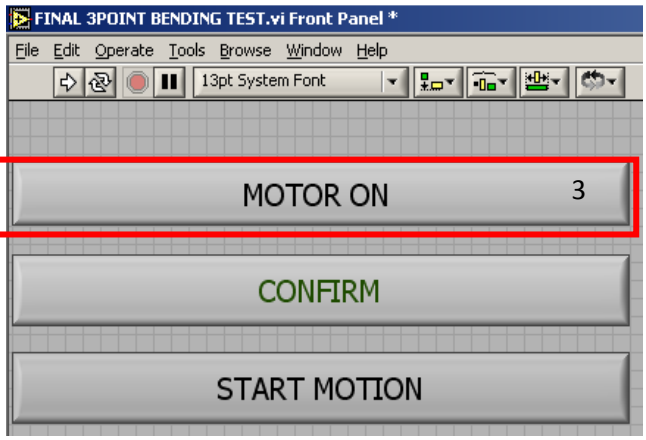

CLICK THE BOX

As soon as the box is clicked, a separate program will pop up

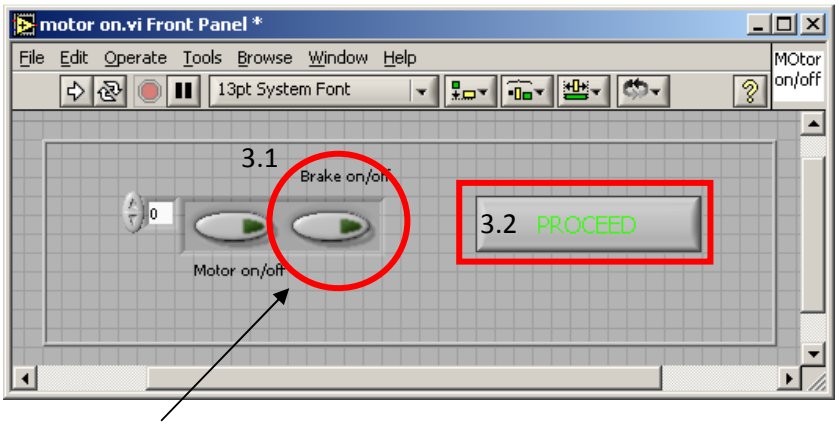

CLICK THIS SWITCH

- ✓ Press the Brake on/off (3.1)
- ✓ This is done to control the motor brake and ensure safety
- ✓ Press PROCEED button (3.2) to close this window and to proceed further

STEP 4: PRESS CONFIRM BUTTON

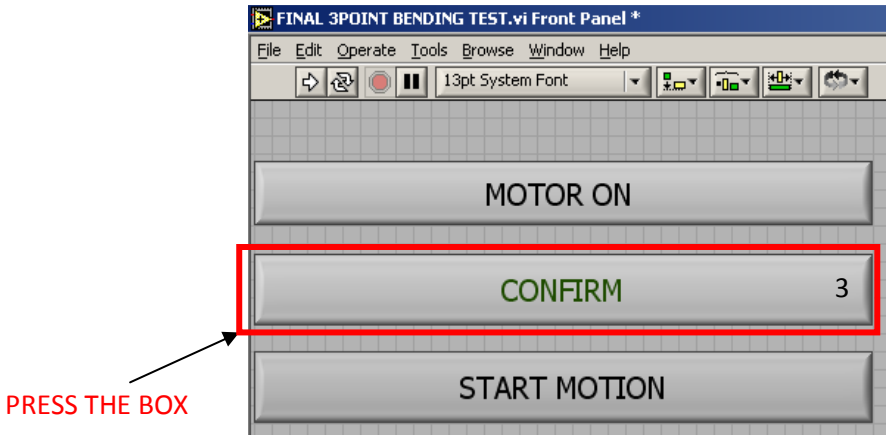

- ✓ If the defined distance and speed values are correct, press the confirm box to proceed further.

STEP 5: PRESS START MOTION

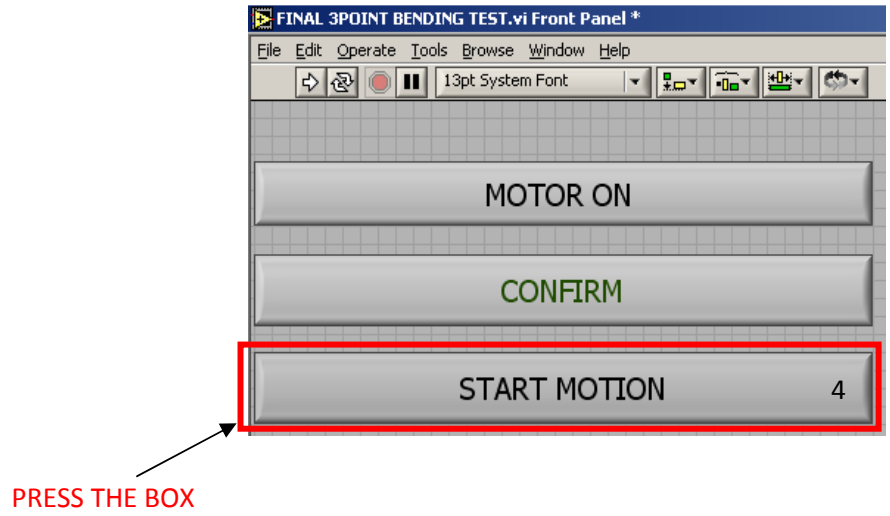

- ✓ As box is pressed the motor will start moving
- ✓ As the striker starts moving, loading measurement will begin.

- ✓ Loading measurement indicated by (9).
- ✓ Unloading measurement indicated by (10).
- ✓ The striker will stop moving after it reaches the specified distance

Six degrees of freedom force and moment values of both sensors

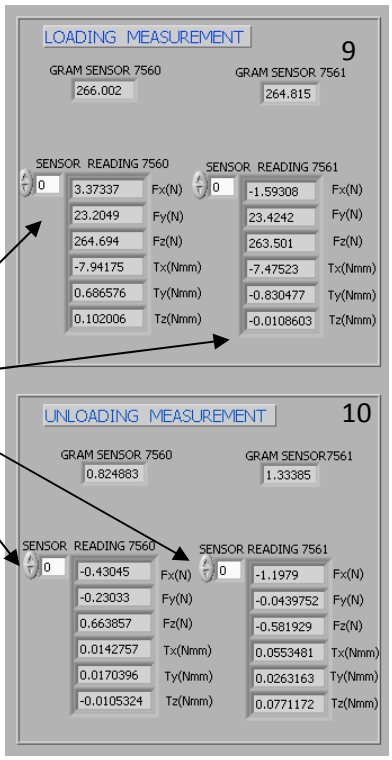

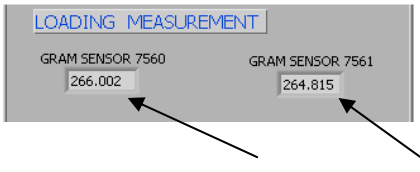

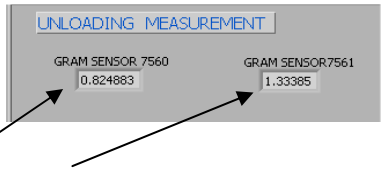

Summation of force of all 3 axes of both sensors in grams

$$\sum F = \sqrt{Fx^2 + Fy^2 + Fz^2} \qquad (1)$$

$$1g = N \times \frac{1000}{9.81} \qquad (2)$$

- ✓ As the Striker stops moving, (6) will indicate the Load/Displacement curve.

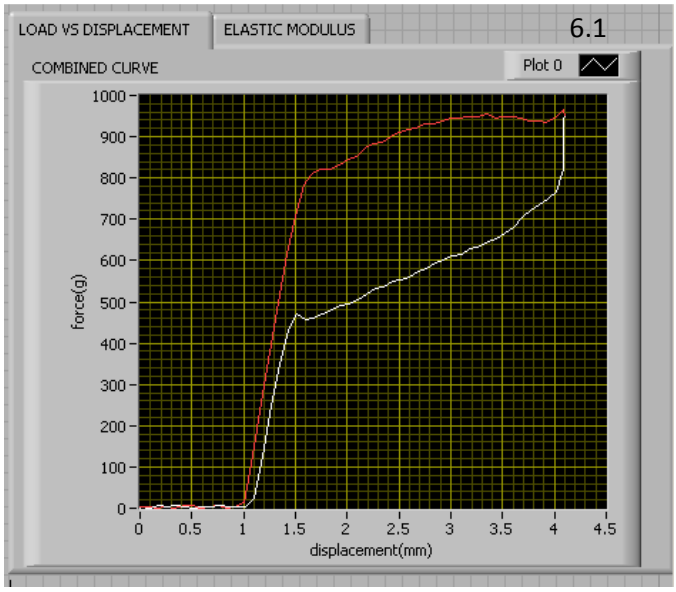

- ✓ By examining the load/displacement curve (6), the point where the force (g) increases linearly is the position where the striker touches the wire.

- ✓ In this example, by analyzing the X axis of the curve (displacement), the force value increases linearly from 1mm to 4.1mm and this verifies that the striker was located 1 mm above the specimen wire.

- ✓ So by analyzing the X axis of the curve, position of the striker above the wire could be determined.

OPTIONAL (Can skip and move to STEP 5):

To calculate the elastic modulus (round wires)

PRESS THIS to go to next page

- Enter the Force value in grams at the peak deflection indicated in LOADING MEASUREMENT block (9)
- Enter the diameter of the round wire in millimeter.
- Enter the peak defection in millimeter.

$$I = \frac{\pi d^4}{64} \qquad (3)$$

$$E = \frac{FL^3}{48I\delta} \qquad (4)$$

- It will give the value of Elastic modulus in Giga Pascal (Gpa).

✓ When STEP 5 is done proceed to STEP 6

STEP 6: STOP MEASUREMENT

PRESS THIS BOX

STEP 6: RESET PROGRAM

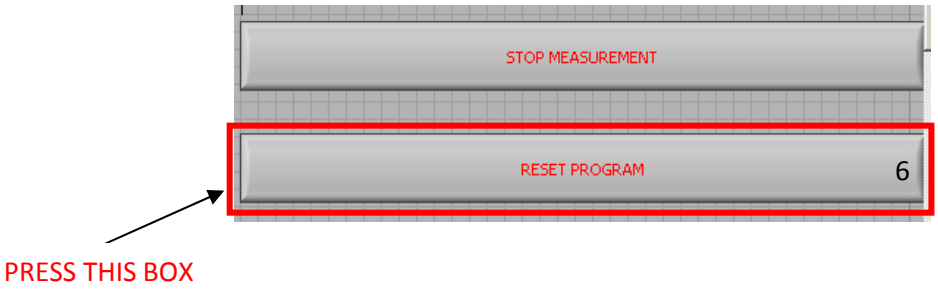

✓ This ends the calibration step.

✓ The real measurement step begins now

✓ Go to STEP 2 and specify the distance and speed values accordingly once the 0 mm location is located. (See flow chart)

- ✓ Once the distance and speed values are specified, go to STEP 3 and press confirm button.

- ✓ Repeat STEP 4, Start motion for performing another test.
- ✓ The program will terminate after the measurement is repeated for 4 times.

6 DATA MANIPULATION

- All the loading and unloading values will be written into text files.

- Follow this path to open the text files **“loading sensor7560.txt”, “loading sensor7561.txt”, “unloading sensor7560.txt”, “unloading sensor7561.txt”.**

C:\Documents and Settings\Wire Test\My Documents\adithya\NEW VIS

- Text files could be copied to excel and all the values will could be manipulated according to the need (Data can be transferred to excel for further manipulations)